

AI-Driven Multiscale Study on the Mechanism of Polygonati Rhizoma in Regulating Immune Function in STAD

Peizheng Yang,[#] Xiangyu Wang,[#] Jianhua Yang,[#] Biaobiao Yan, Haiyang Sheng, Yan Li, Yinfeng Yang,^{*} and Jinghui Wang^{*}



Cite This: *ACS Omega* 2025, 10, 19770–19796



Read Online

ACCESS |



Metrics & More

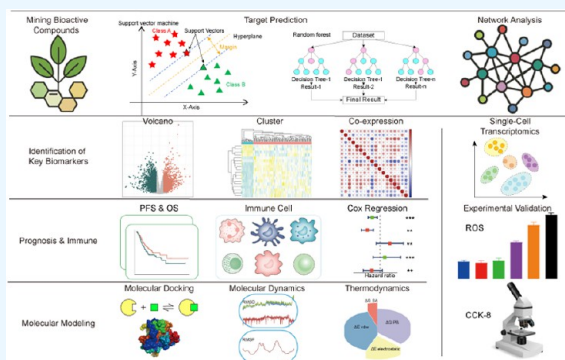


Article Recommendations



Supporting Information

ABSTRACT: Polygonati Rhizoma, a traditional Chinese medicine, has demonstrated immunomodulatory and anticancer properties, yet its precise mechanisms in stomach adenocarcinoma (STAD) remain underexplored. This study aims to uncover the multitarget mechanisms of Polygonati Rhizoma in regulating the tumor immune microenvironment in STAD using artificial intelligence (AI)-driven network pharmacology, bioinformatics, and single-cell RNA sequencing, offering new insights into its immunotherapeutic potential. This study harnessed the power of AI to unravel the molecular mechanisms underlying Polygonati Rhizoma's effects. AI-driven methodologies screened 38 putative constituents, retaining 8 based on ADME criteria. Machine Learning algorithms predicted potential targets, which were cross-referenced with 5,569 immune-related genes from GeneCards, revealing 52 immune-associated targets. Differential expression analysis of the STAD data set identified 18 overlapping DEGs with prognostic significance and immune cell infiltration correlations. Key targets (AKT1, TP53, PTGS2 and VEGFA) emerged as central nodes in the network, with AI-assisted molecular docking confirming strong binding affinities, particularly between diosgenin and these core proteins. Molecular dynamics simulations further validated these interactions. Single-cell RNA sequencing revealed distinct target-gene expression patterns across malignant, stromal, and immune cell subsets in digestive-system tumors. In vitro, Polygonati Rhizoma extract significantly inhibited HGC-27 cell viability and increased intracellular ROS levels. These findings underscore the critical role of AI in integrating multiscale analyses, unveiling a multitarget immunomodulatory and antitumor mechanism for Polygonati Rhizoma in STAD, and providing a foundation for future preclinical and clinical studies.



1. INTRODUCTION

Stomach adenocarcinoma (STAD) is among the most prevalent and lethal malignancies worldwide, ranking as the fifth most common cancer and the third leading cause of cancer-related deaths globally.¹ Despite advancements in diagnostic techniques and therapeutic interventions, the prognosis for advanced STAD remains dismal, with a five-year survival rate below 30%.² This poor outcome is primarily due to late-stage diagnosis, high rates of metastasis, and resistance to conventional therapies.³ Conventional drugs for STAD face numerous limitations in clinical application, including drug resistance, toxic side effects, poor targeting, and high recurrence rates. Long-term chemotherapy often leads to acquired resistance in tumor cells, resulting in reduced therapeutic efficacy. Meanwhile, non-specific cytotoxicity to normal tissues may cause severe gastrointestinal reactions, myelosuppression, and neurotoxicity, significantly impairing patients' quality of life. Moreover, due to the molecular heterogeneity of STAD, patients show varied responses to the same chemotherapy regimen, making precision treatment challenging.⁴ Therefore, novel therapeutic strategies

are urgently needed to improve clinical outcomes and extend patient survival.

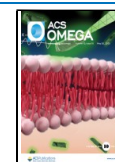
Current treatment options for STAD include surgical resection, chemotherapy, radiotherapy, and emerging targeted and immunotherapies. While surgical intervention is effective for early stage STAD, its utility in advanced or metastatic cases is limited, necessitating systemic chemotherapy or radiotherapy to control disease progression.^{5,6} Targeted therapies, such as trastuzumab for HER2-positive STAD, have made significant strides in personalized medicine, improving outcomes for select patient populations.⁷ Furthermore, immune checkpoint inhibitors targeting the PD-1/PD-L1 axis have shown promise in tumors with high microsatellite instability (MSI-H) or robust PD-L1 expression.⁸ However, these immunotherapies exhibit

Received: February 1, 2025

Revised: April 26, 2025

Accepted: April 30, 2025

Published: May 11, 2025



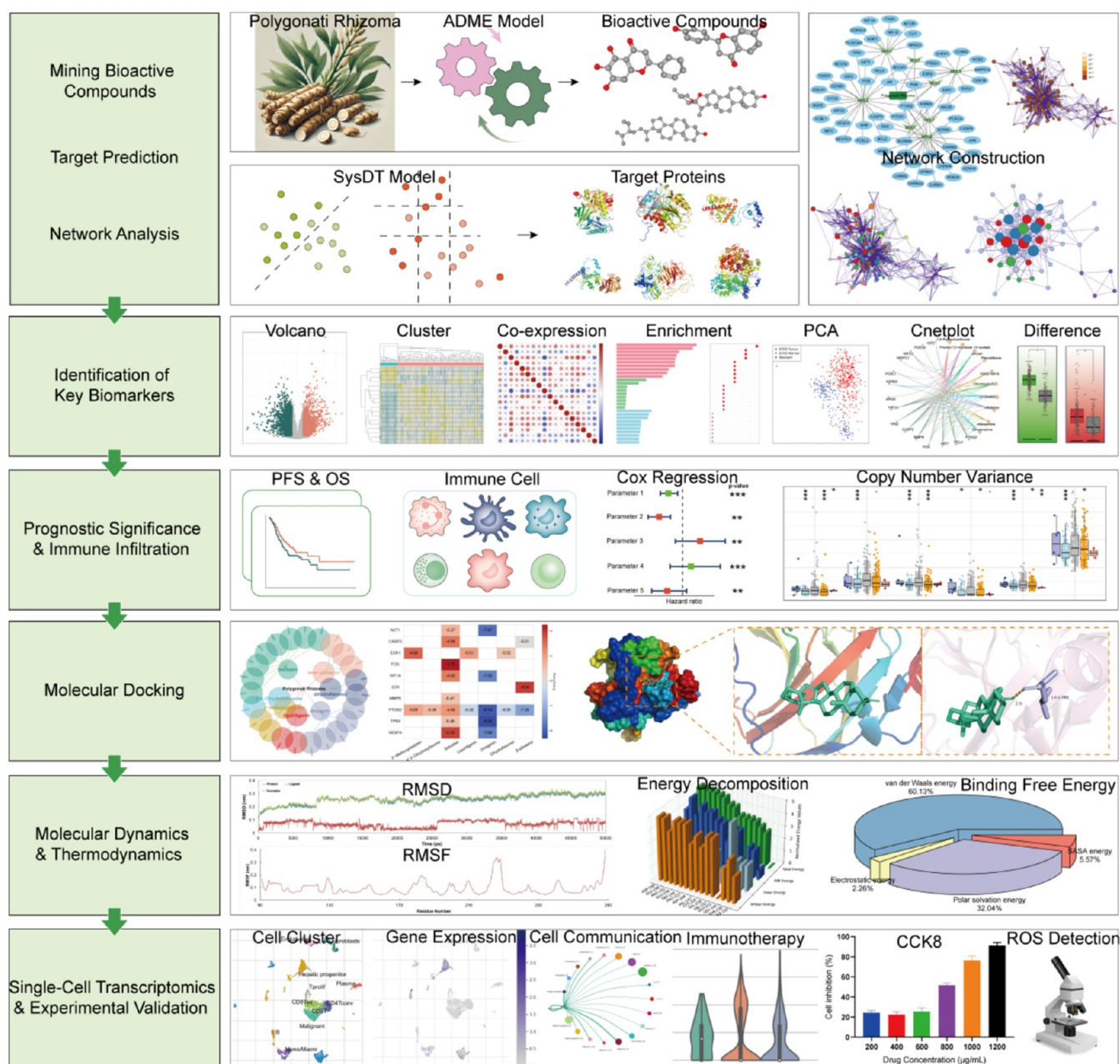


Figure 1. Workflow of the study design.

modest response rates and are often undermined by resistance mechanisms, underscoring the need for novel immunomodulatory agents and combination strategies.⁹

The dynamic interplay between the immune system and cancer cells is crucial in STAD progression and metastasis. Tumor cells exploit various mechanisms to evade immune surveillance, including downregulating major histocompatibility complex (MHC) molecules, secreting immunosuppressive cytokines, and recruiting regulatory T cells (Tregs) and myeloid-derived suppressor cells (MDSCs) into the tumor microenvironment (TME).^{10,11} The composition and functionality of immune cell infiltration within the TME significantly influence patient prognosis and responsiveness to immunotherapy.¹² Elucidating the molecular mechanisms of immune evasion and the roles of immune cell subsets in STAD is vital for advancing immunotherapeutic strategies.¹³

Traditional Chinese Medicine (TCM) has long been utilized as a complementary approach in cancer treatment, targeting multiple biological pathways simultaneously.¹⁴ Polygonati Rhizoma, a widely used herb in TCM, exhibits diverse pharmacological properties, including antioxidant, anti-inflammatory, immunomodulatory, and antitumor activities.¹⁵ Bioactive compounds such as flavonoids, isoflavones, phytosterols, and steroidal saponins have been identified as key contributors to its therapeutic effects.¹⁶ Recent studies have shown that these compounds inhibit cancer cell proliferation, induce apoptosis, suppress angiogenesis, and modulate immune responses, highlighting their potential as adjunctive agents in cancer therapy.^{17,18} Polygonati Rhizoma has been reported to exert immunoregulatory effects primarily by activating the immune system, which includes enhancing the proliferation and functional activity of immune cells, as well as stimulating antibody production. The polysaccharides derived from

Polygonati Rhizoma contribute to humoral immunity by promoting the generation of hemolysin and enhancing the phagocytic capacity of peritoneal macrophages. In addition, its regulatory influence on immune organs, particularly the spleen, has been substantiated. Extracts such as PSE30 and PSE75 were found to significantly enhance the activity of natural killer (NK) cells and upregulate the mRNA expression of Th1- and Th2-associated markers in splenocytes, indicating a dual role in both innate and adaptive immune responses.^{19–2021}

However, the specific molecular mechanisms underlying the immunomodulatory effects of Polygonati Rhizoma in STAD remain to be elucidated. Although previous studies have investigated the pharmacological properties of Polygonati Rhizoma, most research has primarily focused on its broad-spectrum antitumor effects rather than its specific role in modulating the tumor immune microenvironment (TIME) in STAD. Moreover, existing studies predominantly rely on bulk transcriptomics, which lacks the resolution to accurately depict cellular heterogeneity and complex intercellular interactions within the TIME. Advances in artificial intelligence (AI), network pharmacology and bioinformatics have revolutionized the study of TCM, enabling systematic analyses of multi-component, multitarget interactions and facilitating the identification of potential therapeutic mechanisms.²² Additionally, single-cell RNA sequencing (scRNA-seq) has emerged as a powerful tool for deciphering the cellular heterogeneity and immune characteristics of the tumor microenvironment in STAD and other gastrointestinal malignancies.^{23,24} By integrating scRNA-seq analysis across different gastrointestinal tumors, a more comprehensive understanding of the potential role of Polygonati Rhizoma in modulating the immune microenvironment of these malignancies can be achieved.

To address this research gap, our study focuses specifically on STAD, we leverage AI-driven network pharmacology combined with bioinformatics analysis and scRNA-seq to systematically investigate the immunomodulatory mechanisms of Polygonati Rhizoma in STAD, an area that has yet to be systematically explored. Through ADME screening, target prediction algorithms, network construction, molecular docking, molecular dynamics simulations, bioactivity prediction, and experimental validation in the HGC-27 gastric cancer cell line, we aim to elucidate the multitarget action mechanisms of Polygonati Rhizoma, particularly its impact on the TIME. By elucidating key molecular interactions and immunoregulatory pathways, our findings will provide novel insights into the immunotherapeutic potential of Polygonati Rhizoma and contribute to the advancement of precision medicine in STAD. The workflow of the study design see in Figure 1.

2. MATERIALS AND METHODS

2.1. Acquisition of Compound and Disease Targets.

The chemical constituents of Polygonati Rhizoma were systematically retrieved from the Traditional Chinese Medicine Systems Pharmacology Database (TCMSP),²⁵ identifying a set of distinct bioactive compounds. To explore immune-related targets, the GeneCards database²⁶ was queried using the keywords “immunity,” “immune,” and “immunization,” resulting in 5569 immune-associated targets. To ensure relevance, only genes with an immune relevance score exceeding 1 were selected for subsequent analysis. Additionally, human disease-related genes were curated and validated through the UniProt database²⁷ to enhance the reliability of the target data set.

2.2. ADME Screening Model. The pharmacokinetics of drugs in the human body is governed by four key processes: absorption, distribution, metabolism, and excretion (ADME). Early evaluation of ADME properties is essential for predicting pharmacokinetic profiles and minimizing potential drug–drug interactions. As traditional Chinese medicines (TCMs) are predominantly administered orally, oral bioavailability (OB) and drug-likeness (DL) serve as critical parameters in assessing their pharmacokinetic attributes. This study employed an ADME model to evaluate the pharmacokinetics of Polygonati Rhizoma components, with a particular focus on OB and DL.

The oral bioavailability (OB) of the compounds was calculated using the in-house OBioavail 1.1 model,²⁸ which was developed from a data set of 805 structurally diverse drugs. This model demonstrated robust predictive capabilities, with a determination coefficient (R^2) and standard error of estimate (SEE) validated across test sets. The OBioavail 1.1 model incorporated multiple regression techniques, including multiple linear regression (MLR), partial least-squares (PLS), and support vector regression (SVR), to establish optimal variable correlations. To further refine predictions, the spatial variation of adjacent compounds was estimated using the formula

$$\arg \min_n \sum_{i=1}^n \left(\sum_{j=1}^{r_i} \sum_{k=1}^{r_i} \sqrt{(x_j - x_k)^2 / r_i(r_i - 1)} \right) / n \quad (1)$$

Here, n denotes the number of subsets, r_i represents the number of samples in subset i , and x_i and x_k are the descriptor vectors of compounds j and k within subset i . The final Support Vector Regression (SVR) model and the kernel function $K(x, x_i)$ are computed as follows

$$f(x) = \sum_{i=1}^n (\alpha_i - \alpha_i^*) K(x, x_i) + b \quad (2)$$

$$K(x, x_i) = \varphi(x) \cdot \varphi(x_i) \quad (3)$$

The values of DL for the ingredients were computed using the Tanimoto coefficient.²⁹ The formula of calculating DL index is defined as follows

$$T(A, B) = \frac{A \cdot B}{A^2 + B^2 - A \cdot B} \quad (4)$$

where A represents the molecular properties of the TCM components, and B represents the average DL index of all molecules in the drug database.³⁰ Effective components were defined by criteria of $DL \geq 0.18$ and $OB \geq 30\%$.

2.3. Target Prediction Model. SysDT is a comprehensive algorithm that combines random forest (RF) and support vector machine (SVM) methodologies. It facilitates large-scale drug target identification and discovery by integrating chemical, genomic, and pharmacological data.³¹ The classifier in the SVM algorithm is mathematically defined as follows

$$f(x) = \operatorname{sgn} \left(\sum_{i=1}^p a_i y_i k(x_i, x) + b_0 \right) \quad (5)$$

Here, x represents the new object to be classified, and k denotes the kernel function that measures the similarity between two vectors. Candidate target interactions are considered potential targets if their interaction indices exceed 0.8 and 0.7 for the RF and SVM methods, respectively.

2.4. Network Construction. To explore the therapeutic mechanisms of Polygonati Rhizoma, a Drug-Component-Target (D-C-T) network was constructed using Cytoscape.³² The network was derived from compounds identified through ADME screening and targets predicted using the SysDT algorithm.

Cytoscape's bioinformatics tools were utilized for network visualization, enabling a comprehensive analysis of the complex relationships within the data. Heatmaps were employed to visually depict the interactions between components and targets. To identify the most influential components within the networks, two critical topological parameters—degree and betweenness—were calculated using the CentiScaPe 1.2 plugin in Cytoscape.³³

These network-based analyses provide valuable insights into the multicomponent, multitarget interactions that underpin the immunomodulatory and therapeutic effects of Polygonati Rhizoma.

2.5. Biological Function Analysis of Target Proteins. To investigate the biological roles of the identified target proteins, enrichment analyses were performed across three Gene Ontology (GO) categories—Biological Processes (BP), Cellular Components (CC), and Molecular Functions (MF)—as well as Kyoto Encyclopedia of Genes and Genomes (KEGG) pathways. These analyses were conducted using R, with significance thresholds set at a p-value <0.01 and an enrichment factor >1.5. Identified terms were grouped based on their functional similarity to provide a comprehensive overview of the underlying biological mechanisms.

In addition to these analyses, Metascape³⁴ was employed to further explore the biological significance of the gene or protein sets, offering insights into enriched pathways and interconnected functional modules. Furthermore, GeneMANIA³⁵ was utilized to predict gene functions, associations, and interaction networks, enhancing the understanding of functional relationships among targets.

These integrative analyses elucidate the biological pathways and functional networks involved in the therapeutic effects of Polygonati Rhizoma, contributing to a deeper understanding of its immunomodulatory and anticancer mechanisms.

2.6. Molecular Docking. Molecular docking was conducted to validate the immunomodulatory mechanism of Polygonati Rhizoma. Protein sequence information for potential target genes was retrieved from the NCBI database,³⁶ and the longest sequences were selected for homology modeling using SWISS-MODEL.³⁷ Models with the highest GMQE values were evaluated for quality using the Ramachandran plot from SAVES, and those with >90% of residues in allowed regions were considered suitable for docking analysis. Structures of active components were obtained from PubChem³⁸ based on their PubChem CIDs.

The small molecule structures in SDF format were converted to MOL2 format using OpenBabel.³⁹ Macromolecular structures were prepared by removing bound ligands and water molecules. The processed molecules were then imported into AutoDockTools,⁴⁰ where hydrogens were added, charges were calculated, and rigid atom properties were defined. Binding sites were optimized, with lower binding energies indicating more favorable docking interactions.

Docking simulations were performed using a high-precision genetic algorithm. Parameters such as the number of docking runs and random seed generation were optimized to enhance accuracy. The docking model with the lowest binding energy

was selected for further analysis. Visualization of docking results was carried out using PyMOL, highlighting key hydrogen bonds and residues within the docking complexes. This approach ensures a detailed validation of Polygonati Rhizoma's interactions with target proteins, supporting its potential immunomodulatory mechanisms.

2.7. Validation of Compound-Target Interactions via Molecular Dynamics Simulations. Molecular dynamics (MD) simulations were performed to validate the stability and interactions between the core protein and target compounds using the GROMACS 2019.6 software suite⁴¹ with the AmberSB99 force field.⁴² The X-ray crystal structure of protein was retrieved from the Protein Data Bank and used to construct the protein–ligand complexes. These complexes were placed in a cubic simulation box and solvated with SPC/E water molecules to replicate a biological environment.

Long-range electrostatic interactions were computed using the particle mesh Ewald (PME) method, with cutoff distances set to 1.4 nm for van der Waals (vdW) interactions and 1.0 nm for Coulomb interactions.⁴³ Simulations were conducted at 300 K within an NPT ensemble under periodic boundary conditions. System pressure was maintained at 1 bar using the Parrinello–Rahman barostat, with an isothermal compressibility of $4.5 \times 10^{-5} \text{ bar}^{-1}$.⁴⁴

Energy minimization was performed using the steepest descent algorithm for 10,000 steps to resolve steric clashes and optimize the system. This was followed by a 1 ns equilibration simulation to stabilize temperature and pressure conditions, ensuring the system's readiness for the 100 ns production simulation. The production simulation was executed with a 2 fs time step, providing detailed insights into the dynamics and stability of the protein–ligand interactions. This simulation workflow enables robust validation of the interactions, reinforcing the molecular basis of Polygonati Rhizoma's immunomodulatory effects.

2.8. Binding Free Energy Calculations. To evaluate the binding affinities of key bioactive compounds from Polygonati Rhizoma with their respective receptors, the binding free energies of the drug–target complexes were calculated using the g_mmpbsa algorithm, based on the MM/PBSA method.⁴⁵ Furthermore, the energy differences for the drugs, receptors, and drug–target complexes were determined using the following equations.^{46,47}

$$\Delta G_{\text{bind}} = \Delta E_{\text{MM}} + \Delta G_{\text{sol}} - T\Delta S \quad (6)$$

$$\Delta E_{\text{MM}} = \Delta E_{\text{internal}} + \Delta E_{\text{electrostatic}} + \Delta E_{\text{vdw}} \quad (7)$$

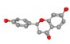
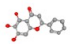
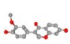
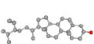
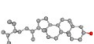
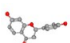
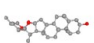
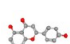
$$\Delta G_{\text{sol}} = \Delta G_{\text{PB}} + \Delta G_{\text{SA}} \quad (8)$$

In which ΔE_{MM} denotes the energy of the drug–protein. ΔG_{sol} , the solvent energy is computed by the sum of polar contribution of ΔG_{PB} (electrostatic solvent free energy) and nonpolar contribution of ΔG_{SA} (nonelectrostatic solvent component), respectively.

2.9. Bioactivity Prediction. Based on the aforementioned MM-PBSA method, the binding free energy was utilized to estimate the biological activity (K_i , μM) of active constituents from Polygonati Rhizoma, thereby evaluating their potential to target the intended protein 06,0.

$$K_i = e^{-\Delta G_{\text{bind}}/RT} \quad (9)$$

Table 1. Effective Components after Removing Target-Free Components

Mol ID	Molecule Name	structure
MOL1	dihydroflavonol	
MOL2	baicalein	
MOL3	3'-Methoxydaidzein	
MOL4	beta-sitosterol	
MOL5	sitosterol	
MOL7	liquiritigenin	
MOL8	diosgenin	
MOL9	4',5-Dihydroxyflavone	

which R represents as the gas constant (1.987×10^{-3} kcal/K-mol) and T (298.15 K) represents to the absolute temperature of the protein–ligand complex.

2.10. Single-Cell Transcriptomic Analysis. Single-cell transcriptomic data sets were obtained from the GEO and TISCH2 databases. Data processing, including quality control, normalization, dimensionality reduction, clustering, differential expression analysis, and data set integration, was performed using the “Seurat” R package. Cell type annotation was conducted with the “SingleR” package based on reference transcriptomic profiles. Gene set enrichment analysis for hallmark pathways was carried out using the “clusterProfiler” package. To infer intercellular ligand–receptor interactions and construct cell–cell communication networks, the “CellChat” package was employed.

2.11. In Vitro Validation Using HGC-27 Gastric Cancer Cells. The HGC-27 gastric cancer cell line was obtained from Wuhan Punosai Life Technology Co., Ltd. Cells were cultured in RPMI 1640 medium supplemented with 10% fetal bovine serum and 1% penicillin/streptomycin. Cultures were maintained under standard conditions at 37 °C in a humidified incubator with 5% CO₂. During the logarithmic growth phase, cells were digested and passaged using 0.25% trypsin to ensure optimal viability and growth.

For experimental treatments, the cells were divided into four groups: a model control group and three Polygonati Rhizoma treatment groups at low (600 μg/mL), medium (800 μg/mL), and high (1000 μg/mL) doses. Each group was exposed to the respective treatments for 24 h to assess the dose-dependent effects of Polygonati Rhizoma on cell viability and other functional assays.

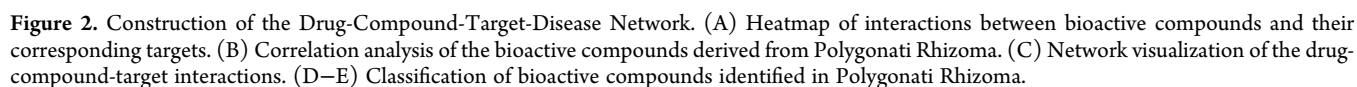
2.12. CCK-8 Cell Viability Assay. According to the manufacturer's protocol, 100 μL of cell suspension was seeded into each well of a 96-well plate and incubated for 24 h under standard cell culture conditions (37 °C, 5% CO₂). Following the incubation period, 10 μL of CCK-8 solution (RCK001, Reed Biotech Ltd., Wuhan, China) was added to each well. The plate was then further incubated for 1 h in the cell culture incubator. After incubation, the absorbance was measured at 450 nm using a microplate reader to assess cell viability.

2.13. Reactive Oxygen Species Detection. In accordance with the manufacturer's instructions, cells were seeded into a 6-well plate and preincubated for 24 h under standard culture conditions (37 °C, 5% CO₂). After treatment with varying concentrations of Polygonati Rhizoma for 24 h, the culture medium was removed, and the ROS detection probe was loaded. DCFH-DA (S0033S-1) was diluted 1:1000 in serum-free medium to achieve a final concentration of 10 μmol/L. One milliliter of this solution was added to each well, and the plate was incubated at 37 °C for 20 min. After incubation, the cells were washed three times with serum-free medium to remove any excess probe. ROS production was then observed under a fluorescence microscope.

3. RESULTS

3.1. Identification of Active Compounds and Target Prediction. A total of 38 active compounds were initially identified for Polygonati Rhizoma using the TCMSP database, with “Polygonati Rhizoma” as the search term. Following this, ADME screening was conducted, and compounds were filtered based on drug-likeness ($DL \geq 0.18$) and oral bioavailability ($OB \geq 30\%$), resulting in the selection of 12 bioactive compounds (Table S1). Target prediction for these bioactive compounds was performed using the SysDT method, which integrates support vector machine (SVM) and random forest (RF) algorithms. This approach allowed for the identification of potential targets for the bioactive compounds.

Four compounds—methylprotodioscin_qt, sibiricoside A_qt, (+)-syringaresinol-O-β-D-glucoside, and zhonghualiaoine 1—were excluded from further analysis due to the lack of predicted targets. Consequently, 8 bioactive compounds were selected for subsequent analyses (Table 1). Figures 2D,E depict the major chemical components of Polygonati Rhizoma and their classifications, which include flavonoids, isoflavones, phytosterols, and steroidal compounds. Flavonoids such as 4',5-Dihydroxyflavone, Liquiritigenin, Dihydroflavonol, and Baicalein are recognized for their antioxidant, anti-inflammatory, and antitumor properties. Isoflavones, such as 3'-Methoxydaidzein, display notable estrogen-like effects. Phytosterols, including Sitosterol and β-Sitosterol, contribute to



steroid hormone synthesis and have been associated with anti-inflammatory and antitumor effects.

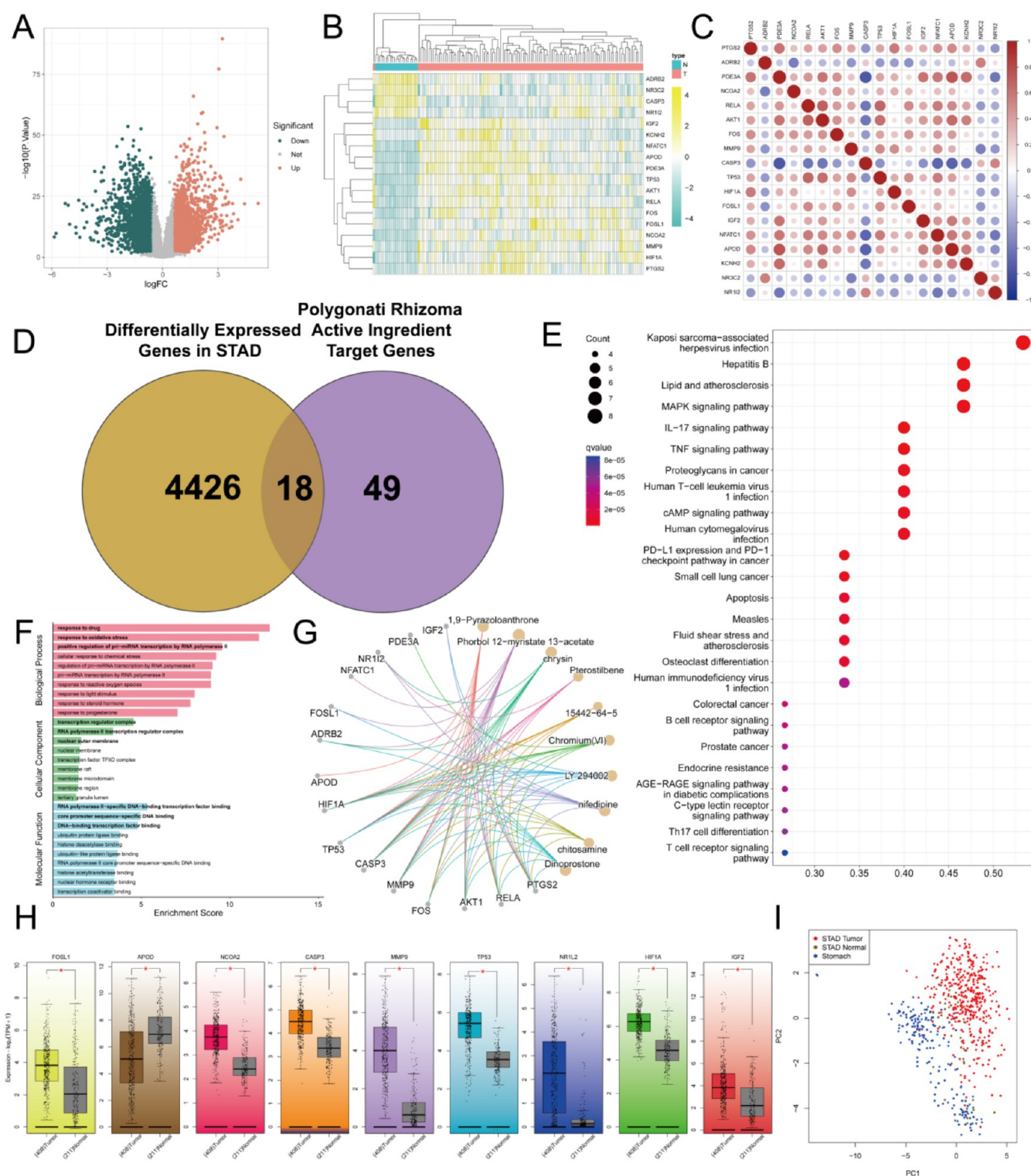


Figure 4. Identification and Functional Analysis of Differential Genes in STAD. (A) Volcano plot of differentially expressed genes (DEGs) in the STAD data set GSE54129. (B) Heatmap of clustering analysis for intersecting genes. (C) Coexpression analysis of intersecting genes. (D) Intersection analysis of DEGs in the STAD data set GSE54129 and target genes of active components from Polygonati Rhizoma. (E) KEGG pathway enrichment analysis of intersecting genes. (F) GO enrichment analysis of intersecting genes. (G) Interaction analysis between intersecting genes and compounds. (H) Differential expression analysis of intersecting genes in tumor and normal tissues. (I) PCA analysis of intersecting genes.

After removing duplicate targets, a total of 67 unique targets were identified (Table S2), providing a solid foundation for further investigation into the molecular mechanisms underlying the immunomodulatory effects of Polygonati Rhizoma bioactive compounds.

3.2. Construction of the Drug-Component-Target-Disease Network. Using data from the 8 bioactive compounds and 67 target genes, a Drug-Component-Target (D-C-T) network (Figure 2C) was constructed using Cytoscape. These networks provide a comprehensive visualization of the

pharmacological effects of Polygonati Rhizoma bioactive compounds.

A clustering heatmap of the compound–target interactions for Polygonati Rhizoma revealed significant interactions between specific compounds, particularly baicalein, diosgenin, 3'-Methoxydaidzein, and β -sitosterol, and their corresponding target genes (Figure 2A). Further evaluation through correlation analysis of these bioactive compounds showed a low degree of intercompound correlation, indicating that these compounds may influence target genes independently rather than acting synergistically (Figure 2B).

These network analyses offer valuable insights into the diverse molecular interactions of Polygonati Rhizoma, laying the groundwork for exploring its therapeutic mechanisms and potential applications.

3.3. Identification of Immune-Related Genes and Construction of the Protein–Protein Interaction Network. To explore the functional roles of the target proteins associated with Polygonati Rhizoma, GeneMANIA was used for functional prediction. The most enriched functions included physical interactions, coexpression, and genetic interactions (Figure 3A). To identify immune-related targets, the GeneCards database was queried using five distinct keywords, resulting in a total of 5,569 immune-related genes after adjusting relevance scores and removing duplicates. By intersecting the 67 targets of Polygonati Rhizoma with these immune-related genes, 52 shared target genes were identified (Figure 3D). These genes are closely associated with critical biological functions such as metabolism, apoptosis, and cell proliferation (Figures 3E,F).

The 52 shared targets were then analyzed using STRING to construct a protein–protein interaction (PPI) network. After removing unconnected nodes, 50 target genes remained, with an average degree value of 17.6. These genes were ranked in descending order based on their degree values. Notably, the top 24 targets—AKT1, JUN, TP53, HIF1A, VEGFA, CASP3, ESRI, FOS, PTGS2, MMP9, MTOR, CASP8, CYCS, RELA, CAT, MAPK14, AR, CASP9, CDKN1A, GSK3B, PGR, CCNB1, CCNA2, and NOS2—had degree values greater than the average degree, suggesting that these may serve as potential core genes underlying the immunomodulatory effects of Polygonati Rhizoma (Figure 3C).

In the drug–compound–target network, analysis of the degree values for the eight bioactive compounds of Polygonati Rhizoma revealed the key compounds involved in immunoregulation. The three compounds with the highest degree values were baicalein, β -sitosterol, and diosgenin, suggesting that these compounds may be the primary contributors to the immunoregulatory effects of Polygonati Rhizoma (Figure 3B).

Subsequent analysis of the 52 shared target genes using Metascape revealed that these genes participate in multiple signaling pathways, with cluster analysis by clustering ID identifying key pathways (Figure 3G). Cancer-related pathways emerged as the most significantly enriched, as shown by the *p*-value analysis (Figure 3H). Further enrichment analysis of protein–protein interactions confirmed that these genes are significantly involved in cancer-related pathways (Figures 3I–M).

3.4. Differential Expression Analysis and Functional Insights of Key Genes in STAD. In the STAD data set GSE54129, differential expression analysis identified a total of 4444 differentially expressed genes (DEGs) (Figure 4A). By intersecting these DEGs with the 67 targets of Polygonati Rhizoma, 18 overlapping genes, including key targets such as

AKT1, PTGS2, and TP53, were identified (Figure 4D). Clustering analysis revealed distinct expression patterns among these 18 genes. Specifically, ADRB2, NR3C2, CASP3, and NR1L2 were predominantly expressed in normal gastric tissues, whereas the remaining 14 genes were enriched in gastric tumor tissues. This differential gene distribution underscores significant transcriptomic differences between tumor and normal tissues, suggesting that these genes may have divergent roles in the pathogenesis and progression of gastric tumors (Figure 4B).

Coexpression analysis revealed that the majority of these 18 genes exhibit positive correlations, indicating their potential synergistic roles in STAD development and progression (Figure 4C). Principal component analysis (PCA) based on the expression profiles of these 18 genes effectively segregated samples into distinct clusters corresponding to stomach tissues, STAD-normal tissues, and STAD tumor tissues. The first two principal components (PC1 and PC2) captured most of the variance, with tumor samples (blue) clearly differentiated from normal tissues (yellow) and stomach tissues (red). These findings highlight a distinct molecular profile of STAD tumor tissues, emphasizing the potential of these 18 genes as biomarkers for distinguishing tumor from nontumor samples in gastric cancer (Figure 4I).

To further explore the functional implications of the identified DEGs, Gene Ontology (GO) enrichment analysis was performed (Figure 4F). The enriched GO terms spanned three categories: Biological Processes (BP), Cellular Components (CC), and Molecular Functions (MF). In the BP category, terms such as “response to drug,” “response to oxidative stress,” and “positive regulation of pri-miRNA transcription by RNA polymerase II” were highly enriched, suggesting the involvement of DEGs in stress response and transcriptional regulation. Within the CC category, terms like “nuclear transcription factor complex” and “RNA polymerase II transcription regulator complex” highlighted the nuclear-centric roles of these genes, particularly in transcription-related activities. In the MF category, enriched terms such as “sequence-specific DNA binding,” “DNA-binding transcription factor binding,” and “RNA polymerase II-specific DNA binding” underscored the central role of these genes in transcriptional regulation.

The interaction network of key target genes and compounds revealed intricate regulatory relationships (Figure 4G). Central nodes such as TP53, AKT1, CASP3, and HIF1A were connected with multiple compounds, including pterostilbene, chrysin, and LY294002. These dense connections suggest that these compounds may modulate crucial biological pathways, particularly those associated with apoptosis, angiogenesis, and inflammation, highlighting their potential therapeutic significance.

KEGG pathway enrichment analysis further demonstrated that the 18 genes are significantly involved in several critical biological pathways (Figure 4E). Notable among these are the “Kaposi sarcoma-associated herpesvirus infection” and “Hepatitis B” pathways, which exhibited the highest enrichment levels, indicating their relevance to virus-associated mechanisms. Pathways linked to inflammation and cancer, such as “Lipid and atherosclerosis,” “MAPK signaling pathway,” “IL-17 signaling pathway,” and “TNF signaling pathway,” were also significantly enriched, emphasizing the role of these genes in inflammatory responses and the tumor microenvironment. Moreover, pathways such as “PD-L1 expression and PD-1 checkpoint pathway in cancer” and “Apoptosis” highlighted their involvement in

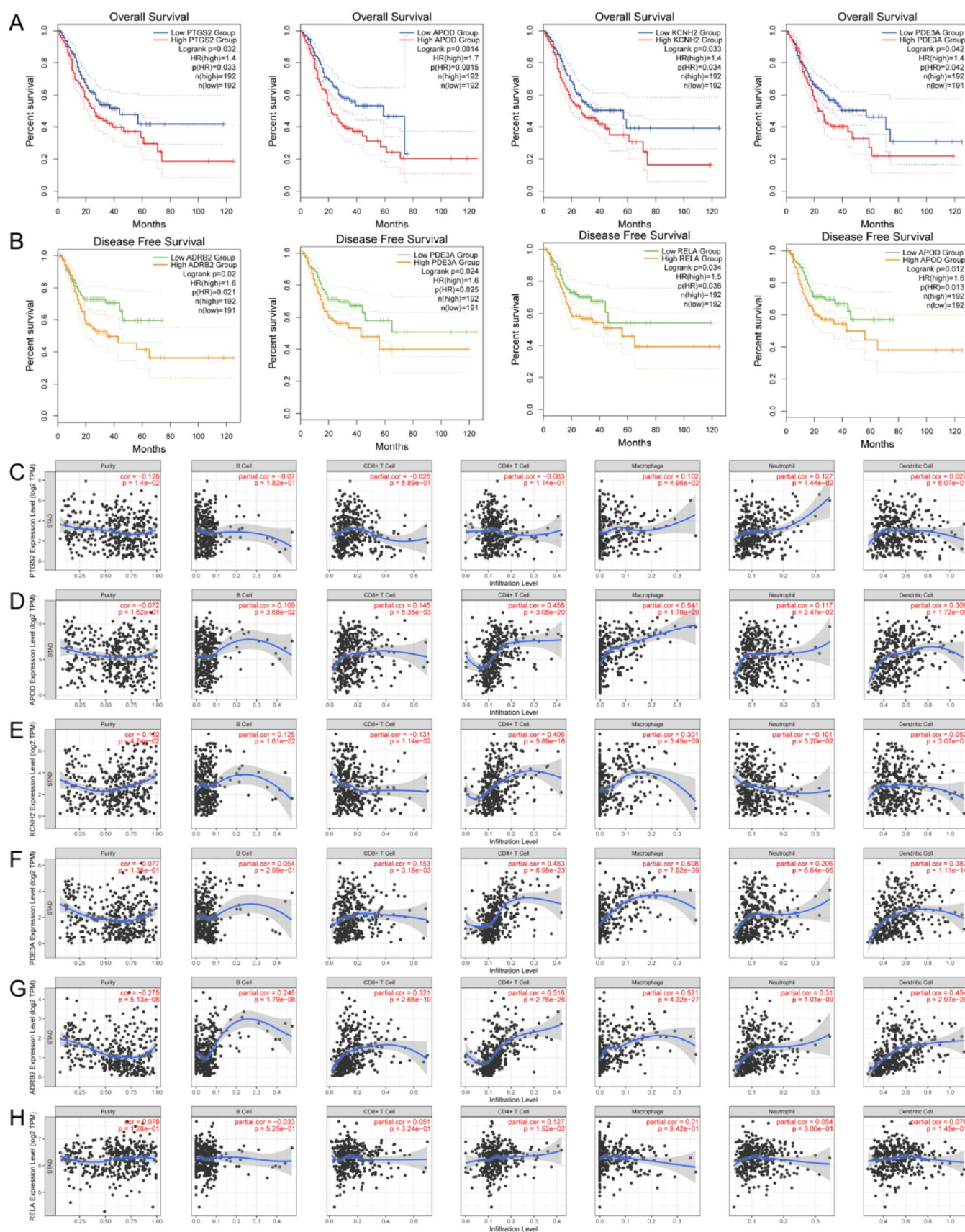


Figure 5. Survival and Immune Infiltration Analysis of Differential Genes in STAD. (A) Overall survival. (B) Disease free survival. (C–H) Correlation analysis between key biomarkers and six types of infiltrating immune cells.

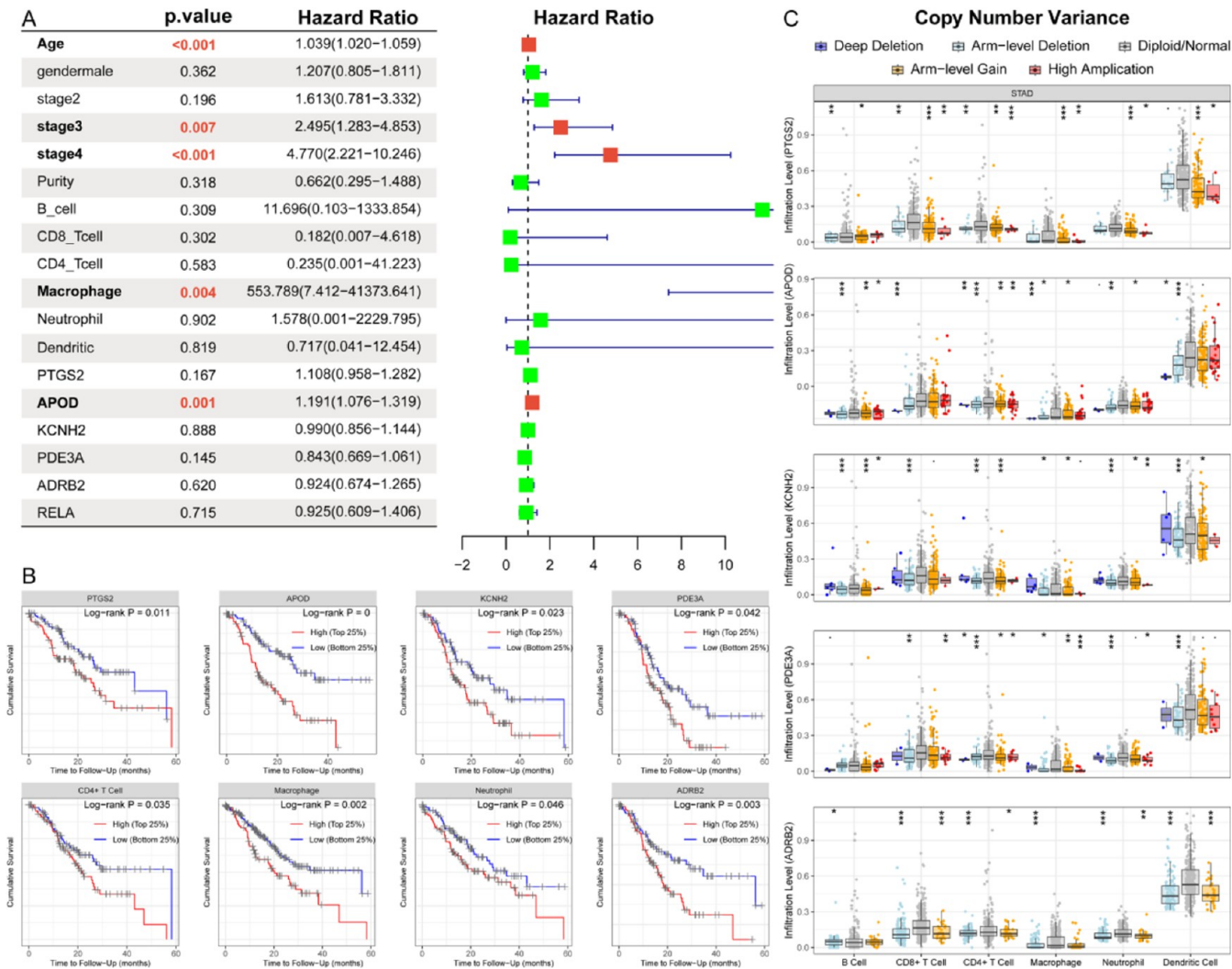


Figure 6. Survival and Immune Infiltration Analysis of Differential Genes in STAD. (A) Multivariate Cox regression model incorporating clinical and immune-related factors, along with key biomarkers. (B) Survival analysis of immune-related factors and key biomarkers. (C) Copy number variation (CNV) analysis of key biomarkers.

immune evasion and cell death regulation. These findings suggest that the identified genes are integral to immune regulation, cancer progression, and inflammation, offering valuable insights into their potential therapeutic and mechanistic roles.

Further analysis revealed that FOSL1, NCOA2, CASP3, MMP3, TP53, NR1L2, HIF1A, and IGF2 were significantly upregulated in gastric tumor tissues compared to normal gastric tissues, whereas APOD was notably downregulated in tumor tissues (Figure 4H).

3.5. Prognostic Significance and Immune Infiltration of Key Genes in STAD. Kaplan–Meier survival analysis revealed that high expression of six intersecting genes—PTGS2, APOD, KCNH2, PDE3A, ADRB2, and RELA—significantly correlated with overall survival (OS) and disease-free survival (DFS) (Figures 5A,B, $P < 0.05$), highlighting their potential as adverse prognostic markers. Scatter plots (Figures 5C–H) further demonstrated significant correlations between biomarker expression and components of the tumor microenvironment (TME), particularly immune cell infiltration, including B cells, CD8+ T cells, CD4+ T cells, macrophages, neutrophils, and dendritic cells. Most of these genes showed positive

associations with the infiltration of these immune cell types, suggesting that they may suppress tumor progression by enhancing immune infiltration. These findings indicate that these biomarkers not only hold prognostic value but also represent novel targets for modulating the TME in STAD, potentially offering new directions for antitumor therapies.

To further assess the prognostic significance of these biomarkers, a multivariate Cox regression model was constructed incorporating gender, clinical stage, tumor purity, six immune cell types, and the six key biomarkers (Figure 6A). The analysis revealed significant associations with survival for several variables, including age ($p < 0.001$, HR = 1.039, 95% CI: 1.020–1.059), stage 3 ($p = 0.007$, HR = 2.495, 95% CI: 1.283–4.853), stage 4 ($p < 0.001$, HR = 4.770, 95% CI: 2.221–10.246), and macrophage infiltration ($p = 0.004$, HR = 553.789, 95% CI: 7.412–41373.641). These variables were identified as potential prognostic indicators. Conversely, gender, tumor purity, immune cell populations (B cells, CD8+ T cells, CD4+ T cells, neutrophils, and dendritic cells), and several genes (PTGS2, APOD, KCNH2, PDE3A, ADRB2, and RELA) did not show a statistically significant association with survival outcomes. Among the genes analyzed, only APOD demon-

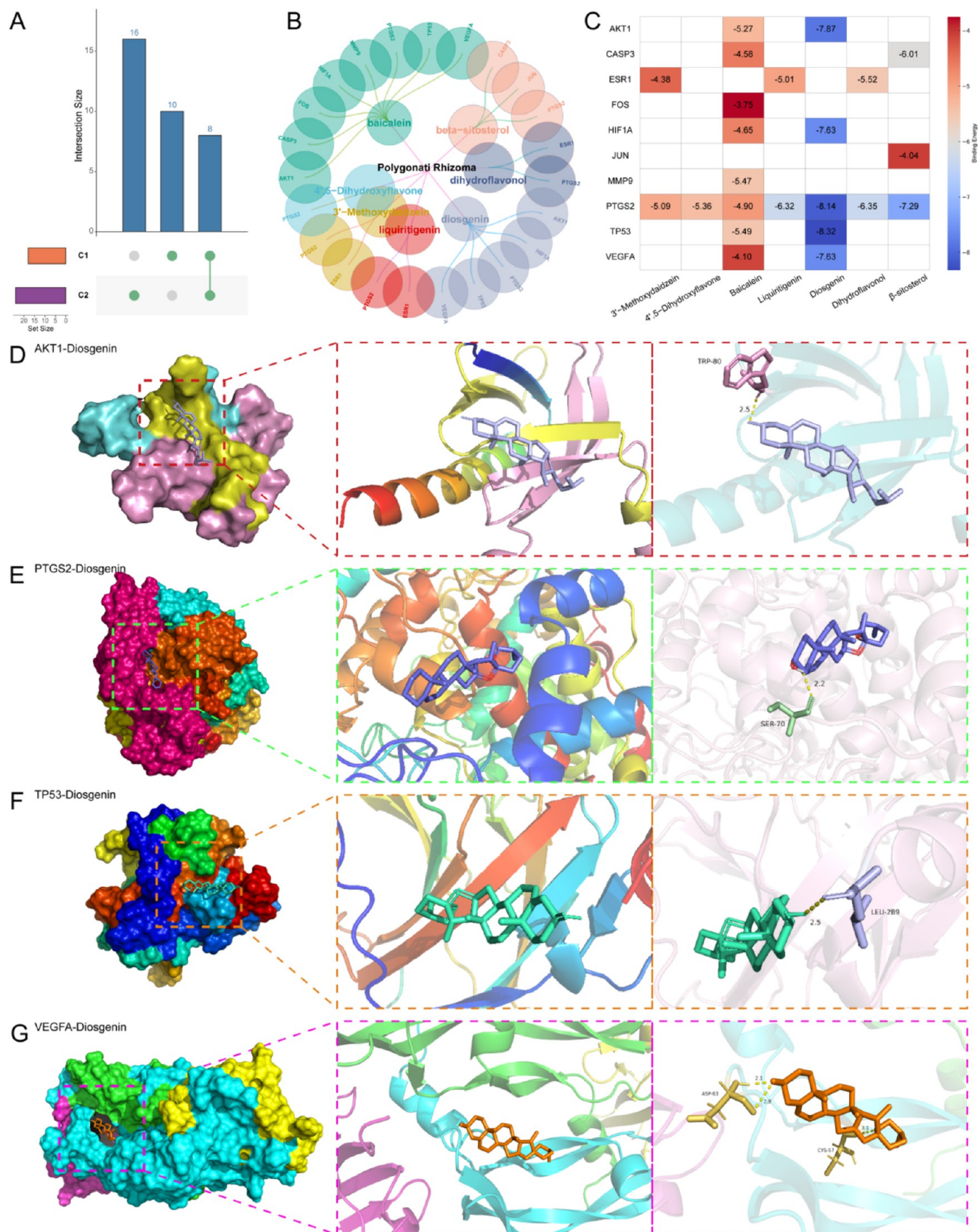


Figure 7. Molecular Docking Results and Visualization. (A) Identification of potential key genes for Polygonati Rhizoma's immune regulatory effects in gastric cancer. c1: intersection between DEGs in STAD and Polygonati Rhizoma. active ingredient target genes. c2: potential core genes of Polygonati Rhizoma in immune regulation. (B) Molecular docking combinations. (C) Energy analysis of molecular docking. The results of molecule docking of AKT1-diosgenin (D), PTGS2-diosgenin (E), TP53-diosgenin(F), VEGFA-diosgenin (G).

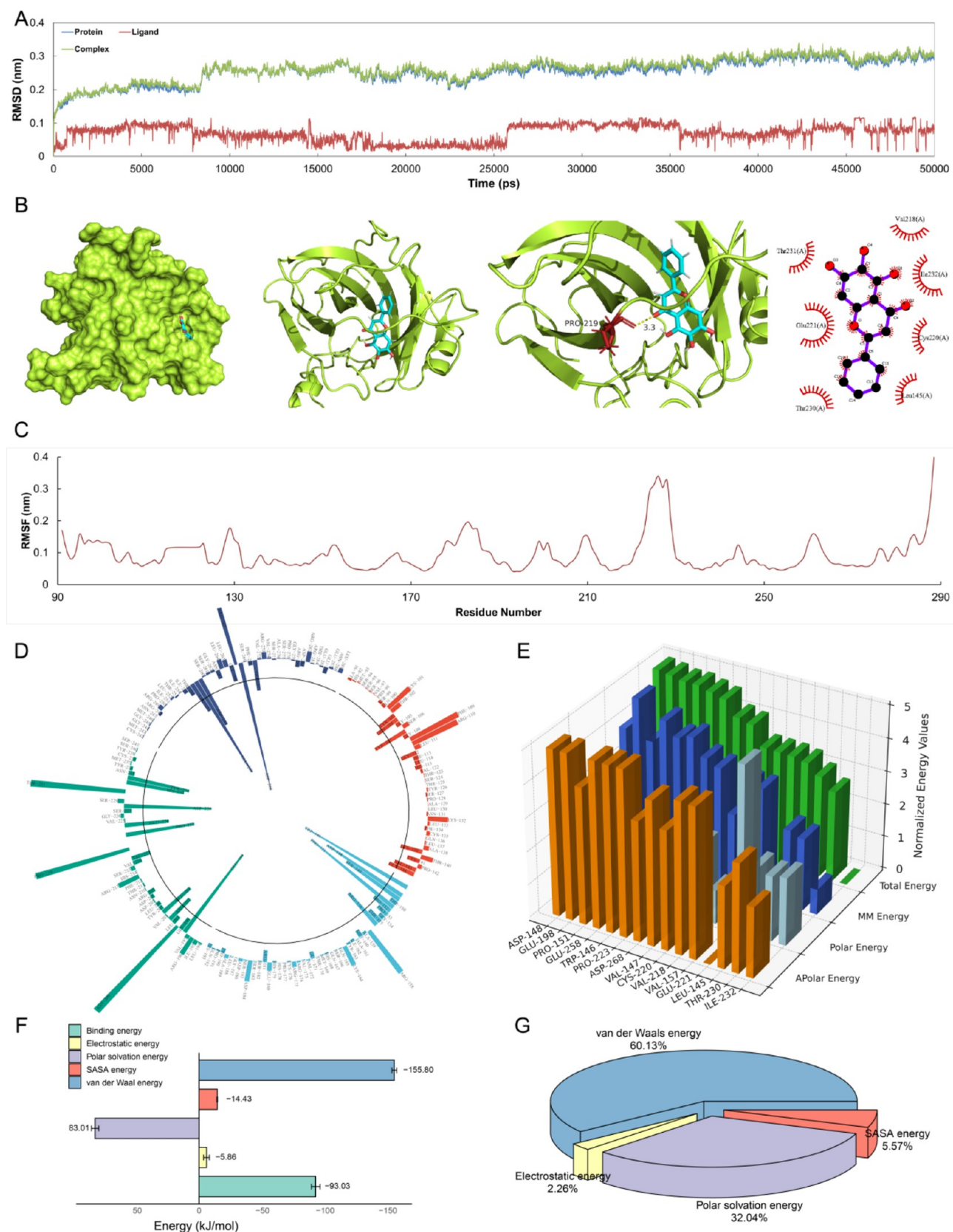


Figure 8. Molecular Dynamics Simulation and Binding Free Energy Calculation. (A) RMSD variation trends of the protein, ligand, and protein–ligand complex during molecular dynamics simulation. (B) Binding mode of the protein–ligand complex at the equilibrium state of molecular dynamics simulation. (C) RMSF variation trends of amino acid residues during molecular dynamics simulation. (D–E) Energy decomposition and distribution of amino acid residues during molecular dynamics simulation. (F–G) Binding free energy analysis based on the MM-PBSA method.

strated a notable association with prognosis ($p = 0.001$, HR = 1.191, 95% CI: 1.076–1.319). These results highlight the strong prognostic relevance of advanced tumor stages (stages 3 and 4) and macrophage infiltration, which could serve as critical factors in predicting survival outcomes.

Kaplan–Meier survival analysis further explored the association between various factors and patient survival outcomes, with patients stratified into high (top 25%) and low (bottom 25%) expression groups for each variable (Figure 6B). Significant survival differences were observed between high and low expression groups for several factors, including PTGS2 (log-rank $p = 0.011$), APOD (log-rank $p < 0.001$), KCNH2 (log-rank $p = 0.023$), PDE3A (log-rank $p = 0.042$), CD4+ T cells (log-rank $p = 0.035$), macrophages (log-rank $p = 0.002$), neutrophils (log-rank $p = 0.046$), and ADRB2 (log-rank $p = 0.003$). In particular, higher expression of APOD, macrophages, and ADRB2 was associated with worse survival, as evidenced by the shorter survival times in the high-expression groups. Conversely, lower expression of certain factors, such as PTGS2 and CD4+ T cells, was associated with better survival outcomes. These findings suggest that these factors may play critical roles in influencing patient prognosis and could serve as potential biomarkers for survival prediction in this cohort. Further studies are warranted to elucidate the underlying mechanisms driving these associations.

Copy number variation (CNV) analysis revealed the relationship between CNV types and immune cell infiltration levels for PTGS2, APOD, KCNH2, PDE3A, and ADRB2 (Figure 6C). The CNV types included deep deletion, arm-level deletion, diploid/normal, arm-level gain, and high amplification. Significant differences in immune cell infiltration were observed for specific CNV types. PTGS2 showed a strong association between high amplification and increased infiltration of macrophages, CD8+ T cells, and neutrophils ($p < 0.05$). APOD exhibited significantly higher infiltration levels of macrophages and CD8+ T cells in cases of arm-level gain and high amplification ($p < 0.01$). KCNH2 demonstrated a notable correlation between deep deletion and reduced infiltration of CD4+ T cells and dendritic cells ($p < 0.05$). PDE3A showed significant infiltration changes in CD8+ T cells and neutrophils under arm-level deletion and high amplification ($p < 0.01$). ADRB2 was linked to increased macrophage infiltration with high amplification and arm-level gain ($p < 0.01$). These findings suggest that CNVs play a critical role in modulating immune cell infiltration, with high amplification and arm-level gain generally promoting higher infiltration, while deep deletion or arm-level deletion is associated with reduced infiltration. These insights emphasize the immunological impact of CNVs on the tumor microenvironment.

3.6. Molecular Docking. To investigate the potential molecular mechanisms underlying the effects of Polygonati Rhizoma in STAD, this study analyzed the intersection between differentially expressed genes (DEGs) in STAD targeted by the active ingredients of Polygonati Rhizoma (C1) and its potential core genes involved in immune regulation (C2). The results revealed that C1 and C2 shared a total of 8 overlapping genes, suggesting that these overlapping genes may play significant biological roles and serve as potential key genes for the immune-regulatory effects of Polygonati Rhizoma in gastric cancer (Figure 7A).

Following this, representative genes were selected for molecular docking studies. Based on the Drug-Component-Target network, a total of 23 molecular docking combinations

were identified (Figure 7B). The docking simulations were conducted with 50 docking runs per combination. The final results were obtained using AutoDockTools, with the minimum binding energy calculated for each docking combination.

The molecular docking results indicated that the binding energy for key active components in Polygonati Rhizoma and core targets was less than -1.2 kcal/mol, suggesting that receptor–ligand binding was spontaneous and the docking interactions were feasible (Figure 7C). A lower binding energy correlates with stronger binding affinity, while a higher binding energy reflects weaker affinity. Analysis of the docking results revealed that the core active components exhibited strong binding energy with key targets, demonstrating the multi-component, multitarget nature of traditional Chinese medicine's clinical efficacy.

From the molecular docking results heatmap, diosgenin emerged with the lowest binding energy and the highest affinity. Diosgenin was found to bind effectively to the active sites of proteins AKT1, PTGS2, TP53, and VEGFA, forming stable interactions through hydrogen bonds with these proteins, contributing to its high affinity and strong binding capacity (Figures 7D–G).

3.7. Molecular Dynamics Simulation and Binding Free Energy Calculation. Molecular docking provides initial structural insights into ligand–receptor interactions; however, its static nature does not fully capture the dynamic behavior and stability of molecular interactions. To validate the reliability of molecular docking and further evaluate the binding free energy of ligand–receptor complexes, this study incorporated Molecular Dynamics (MD) simulation and binding free energy calculation techniques. TP53, a classical tumor suppressor protein frequently mutated or inactivated in cancers, was selected as a key target for anticancer therapies.⁴⁸ Baicalein, one of the major active components of Polygonati Rhizoma,⁴⁹ demonstrated excellent docking scores with TP53, making it an ideal candidate for MD simulation studies to investigate their dynamic interactions and binding stability in greater detail.^{50,51}

The structural stability of the protein, ligand, and their complex during a 50,000 ps (50 ns) MD simulation was evaluated using root-mean-square deviation (RMSD) analysis (Figure 8A). The results indicated that the TP53 protein exhibited slight fluctuations during the initial phase of the simulation (0–5000 ps), followed by stabilization, with an average RMSD maintained at approximately 0.25–0.30 nm. This suggests that the protein structure remained relatively stable throughout the simulation. Baicalein's RMSD was significantly lower (approximately 0.05–0.10 nm), indicating that the ligand maintained a stable conformation. For the TP53–baicalein complex, the RMSD increased gradually during the early simulation phase and subsequently stabilized, mirroring the RMSD trend of TP53, ultimately stabilizing at around 0.25–0.30 nm. These findings suggest that ligand binding did not induce significant perturbations in the protein structure. Overall, the RMSD analysis indicates good stability for the protein–ligand complex during the 50 ns simulation, implying a stable binding conformation between baicalein and TP53. Upon reaching equilibrium, baicalein was observed to interact with the active binding site of the TP53 protein through hydrogen bonding with the active residue PRO-219 (Figure 8B).

Root mean square fluctuation (RMSF) analysis was further conducted to assess the flexibility of individual residues in the TP53 protein during the MD simulation (Figure 8C). The RMSF values, plotted against residue numbers, reveal atomic

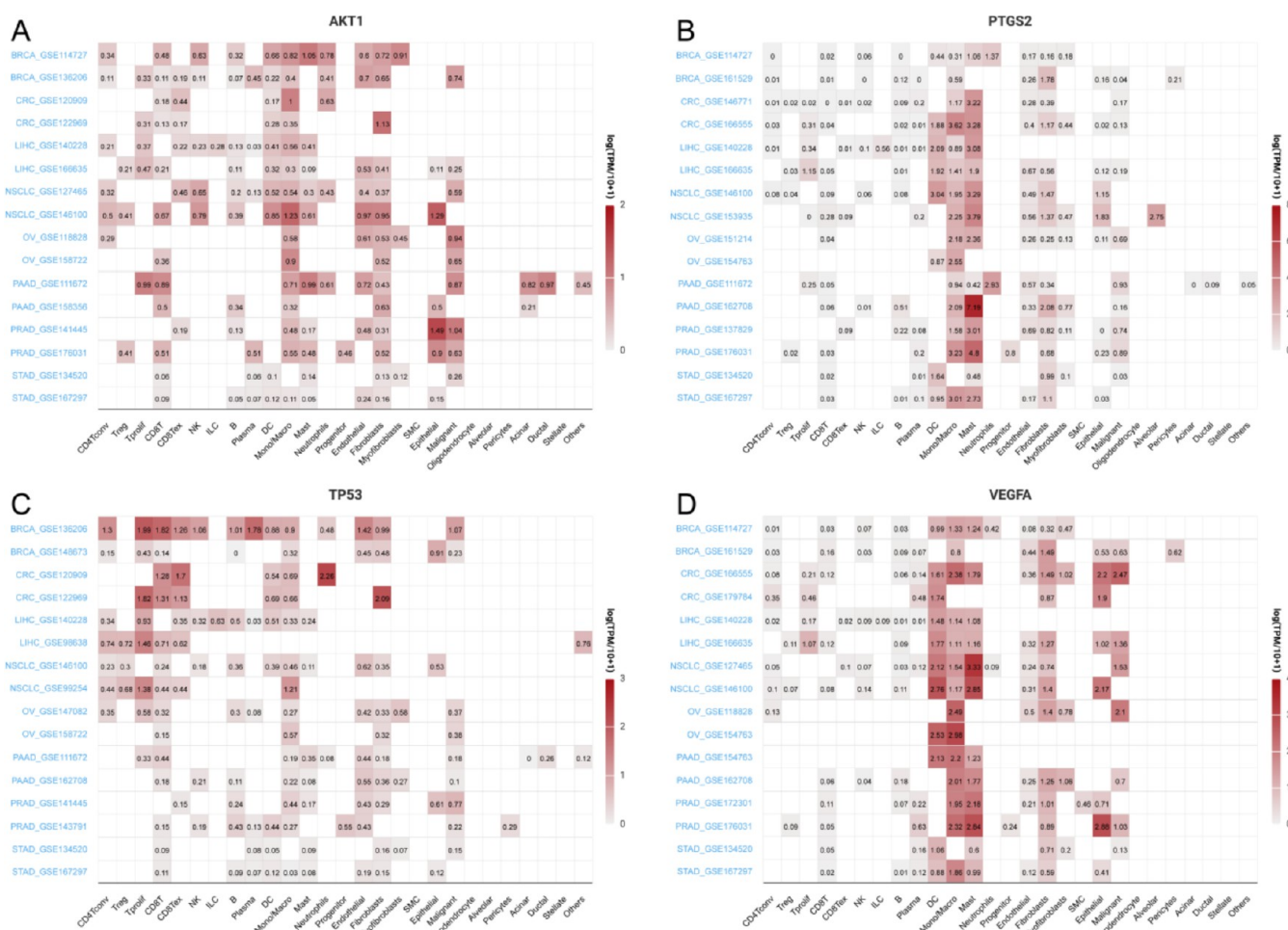


Figure 9. Correlation Analysis of Drug Targets and Immune Cell Infiltration in Eight Common Cancer Types. (A) AKT1-immune infiltration. (B) PTGS2-immune infiltration. (C) TP53-immune infiltration. (D) VEGFA-immune infiltration. The heatmap displays the correlation coefficients between the expression of key targets (AKT1, PTGS2, TP53, VEGFA) and various immune cell infiltration levels across eight common cancers. The color gradient indicates the strength of the correlation (red: positive, blue: negative). The numbers represent the correlation coefficients.

fluctuations for each residue throughout the simulation. Most residues exhibited low RMSF values (<0.2 nm), suggesting these regions were structurally stable, likely located in the protein core or conserved structural domains. Notably, residues beyond position 210 showed significantly elevated RMSF values (>0.3 nm), suggesting higher flexibility in these regions, typically corresponding to loop structures, terminal regions, or solvent-exposed segments of the protein. The RMSF values in the 130–170 residue region were moderate (0.1–0.2 nm), indicating a balance between stability and conformational flexibility. This balance may be critical for ligand binding and dynamic interactions. Overall, RMSF analysis highlights the stability of TP53 while identifying flexible regions that could play important roles in functional changes or ligand interactions.

During the MD simulation, the molecular mechanics (MM) energy, polar energy, nonpolar energy, and total energy of individual amino acid residues were analyzed (Figure 8D). The results showed that the MM energy of most residues was negative, indicating stability in the system. Notably, the MM energy of LIG-290 was -80.77 kcal/mol, with a total energy of -51.25 kcal/mol, suggesting a tendency toward a stable conformation. Residues GLU-221 and GLU-258 contributed significantly to polar energy, with values of 9.56 kcal/mol and -1.22 kcal/mol, respectively, emphasizing their roles in polar

interactions. The energy distribution of amino acid residues was diverse, with certain residues significantly influencing the system's overall stability. The lowest total energy was observed in residues such as ILE-232, THR-230, and LEU-145, among 16 identified residues (Figure 8E). These findings suggest that the system's stability is mainly governed by ligand interactions, both polar and nonpolar. Hydrophobic interactions of nonpolar residues also help maintain equilibrium, providing valuable insights into molecular interactions and optimization for molecular design.

The MM/PBSA (Molecular Mechanics/Poisson–Boltzmann Surface Area) method was employed to estimate the binding free energy of the system. By decomposing the polar and nonpolar energy contributions, MM/PBSA analysis provided direct evidence of the driving forces behind ligand–receptor binding. The results revealed that nonpolar interactions, particularly van der Waals forces, predominantly drive the binding process, while the polar solvation effect negatively impacted binding (Figures 8F,G). This suggests that enhancing nonpolar interactions and optimizing polar groups could improve the ligand's binding affinity. These thermodynamic findings offer a deeper understanding of the molecular mechanisms behind ligand–receptor interactions and serve as a basis for further rational design and optimization of ligands.

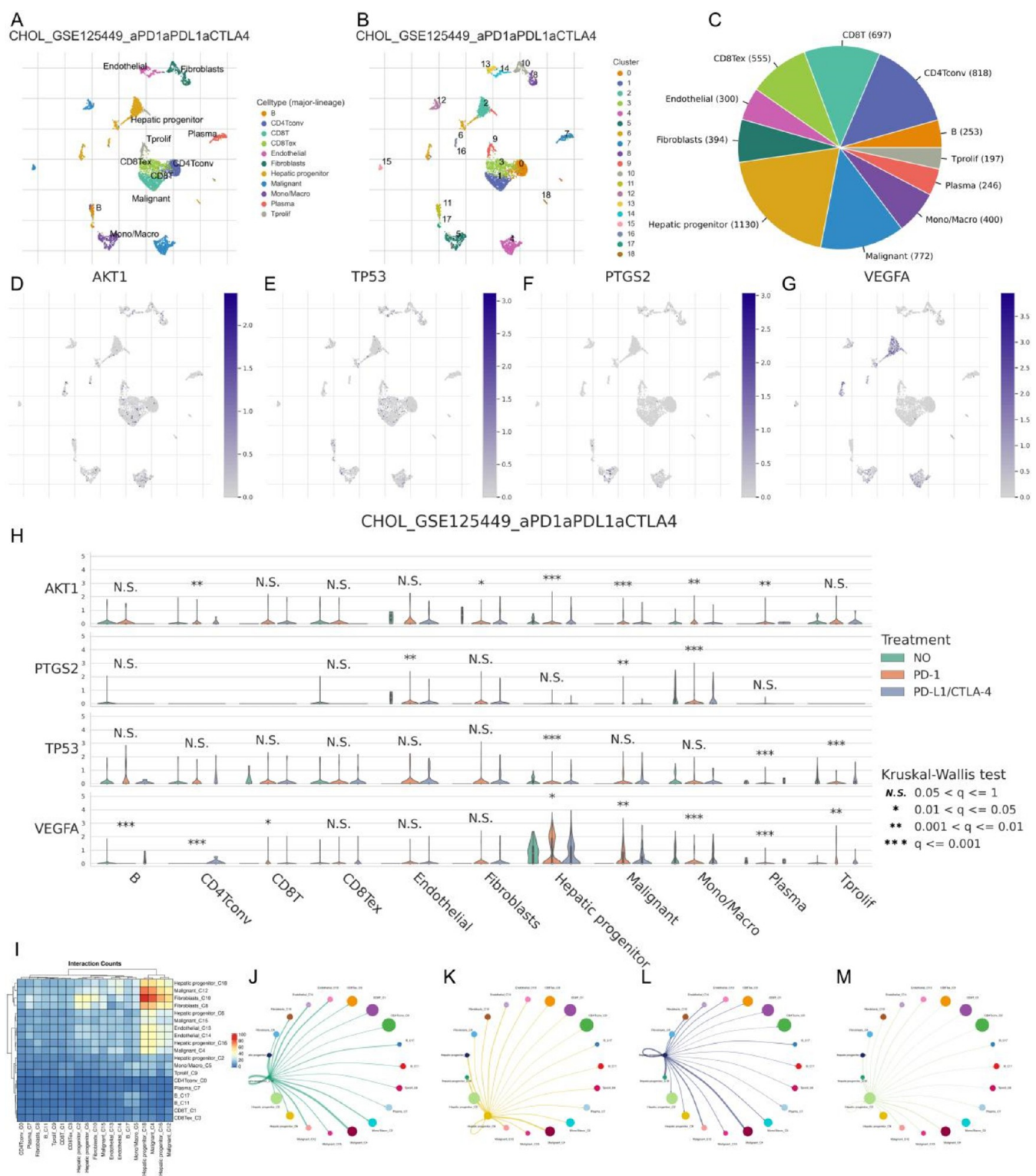


Figure 10. Single-Cell Analysis of CHOL_GSE125449. (A) t-SNE plot displaying cell clustering in CHOL_GSE125449. (B–C) Annotated cell types highlighting major cell lineages in CHOL_GSE125449. (D–G) AKT1, TP53, PTGS2 and VEGFA gene expression across different cell clusters in CHOL_GSE125449. (H) Immunotherapy analysis in CHOL_GSE125449. (I–M) Cell-cell interaction networks in CHOL_GSE125449.

3.8. Correlation Analysis of Key Targets with Immune Infiltration across Multiple Cancers. Previous analyses indicated that the active components of Polygonati Rhizoma target multiple cancer-related pathways. To further explore the potential immunomodulatory roles of these targets, we utilized the TISCH2 database to examine the correlation between the

expression of AKT1, PTGS2, TP53, and VEGFA and immune infiltration levels across eight common cancer types.

The analysis revealed significant positive correlations between AKT1 expression and immune cell infiltration in cancers such as breast cancer and hepatocellular carcinoma, particularly with an increased infiltration of CD8+ T cells and macrophages (Figure

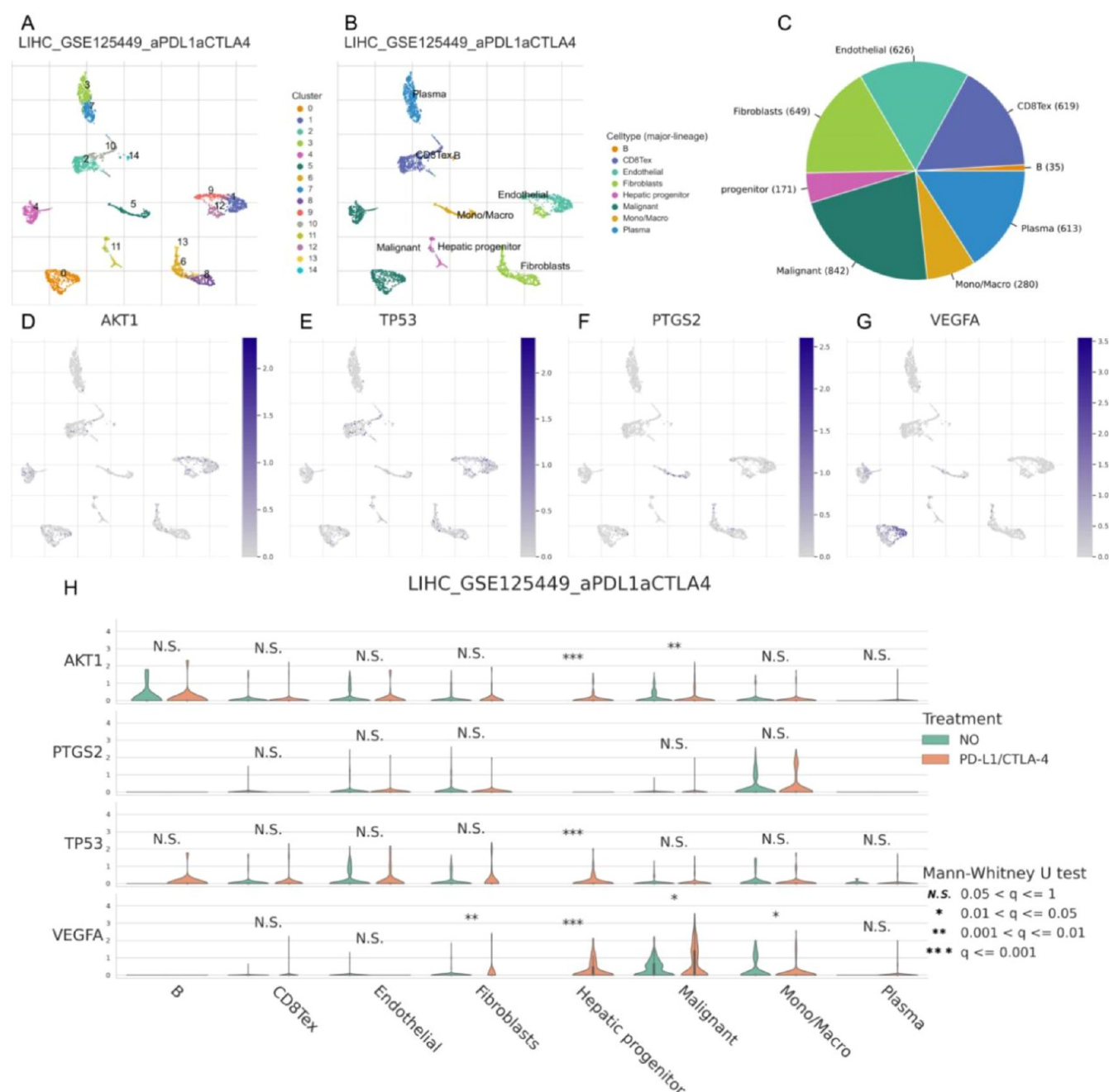


Figure 11. Single-Cell Analysis of LIHC_GSE125449. (A) t-SNE plot displaying cell clustering in LIHC_GSE125449. (B, C) Annotated cell types highlighting major cell lineages in LIHC_GSE125449. (D–G) AKT1, TP53, PTGS2 and VEGFA gene expression across different cell clusters in LIHC_GSE125449. (H) Immunotherapy analysis in LIHC_GSE125449.

9A). These findings suggest that AKT1 plays a crucial role in modulating the tumor immune microenvironment. PTGS2 expression was strongly associated with increased infiltration of pro-inflammatory immune cells, including neutrophils and M1 macrophages, especially in colorectal cancer and pancreatic cancer (Figure 9B). This suggests that PTGS2 may contribute to a pro-inflammatory tumor microenvironment, which could facilitate tumor progression.

A differential immune infiltration pattern was observed for TP53 across various cancer types. In lung adenocarcinoma, TP53 expression was inversely correlated with regulatory T cells, whereas in gastric cancer, a positive association with M1 macrophages was evident (Figure 9C). These results highlight

TP53's dual role in tumor suppression and immune modulation. VEGFA showed strong correlations with immune cell infiltration in highly vascularized tumors, such as renal cell carcinoma and glioblastoma (Figure 9D). Elevated VEGFA levels were linked to increased infiltration of myeloid-derived suppressor cells (MDSCs), suggesting that VEGFA may promote an immunosuppressive microenvironment.

Overall, these findings provide robust evidence that AKT1, PTGS2, TP53, and VEGFA not only participate in cancer progression but also modulate the immune microenvironment in a cancer-type-specific manner. These results underscore their potential as therapeutic targets for enhancing antitumor immunity and improving cancer treatment outcomes.

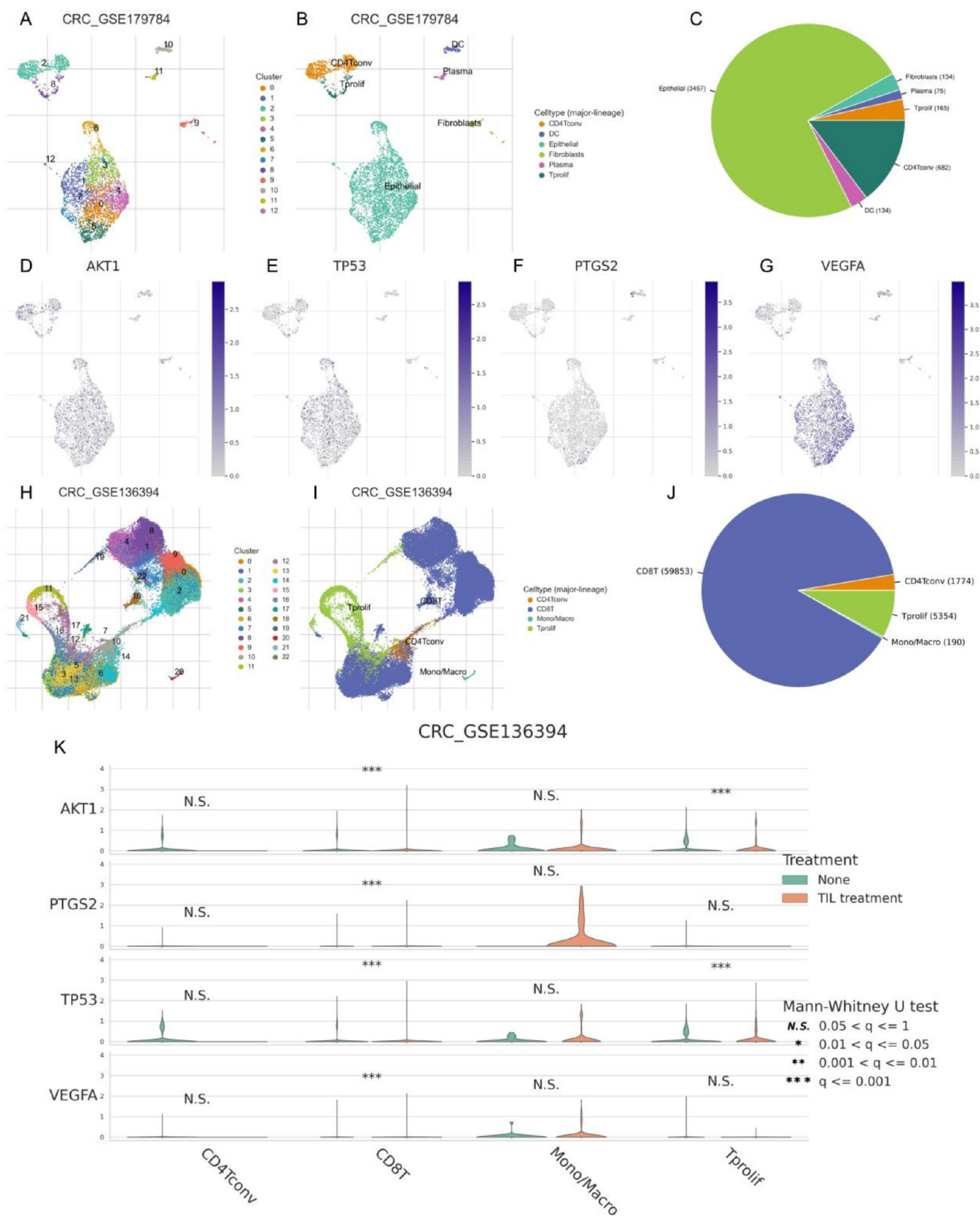


Figure 12. Single-Cell Analysis of CRC_GSE179784 and CRC_GSE136394. (A) t-SNE plot displaying cell clustering in CRC_GSE179784. (B, C) Annotated cell types highlighting major cell lineages in CRC_GSE179784. (D–G) AKT1, TP53, PTGS2 and VEGFA gene expression across different cell clusters in CRC_GSE179784. (H) t-SNE plot displaying cell clustering in CRC_136394. (I, J) Annotated cell types highlighting major cell lineages in CRC_136394. (K) Immunotherapy analysis in CRC_136394.

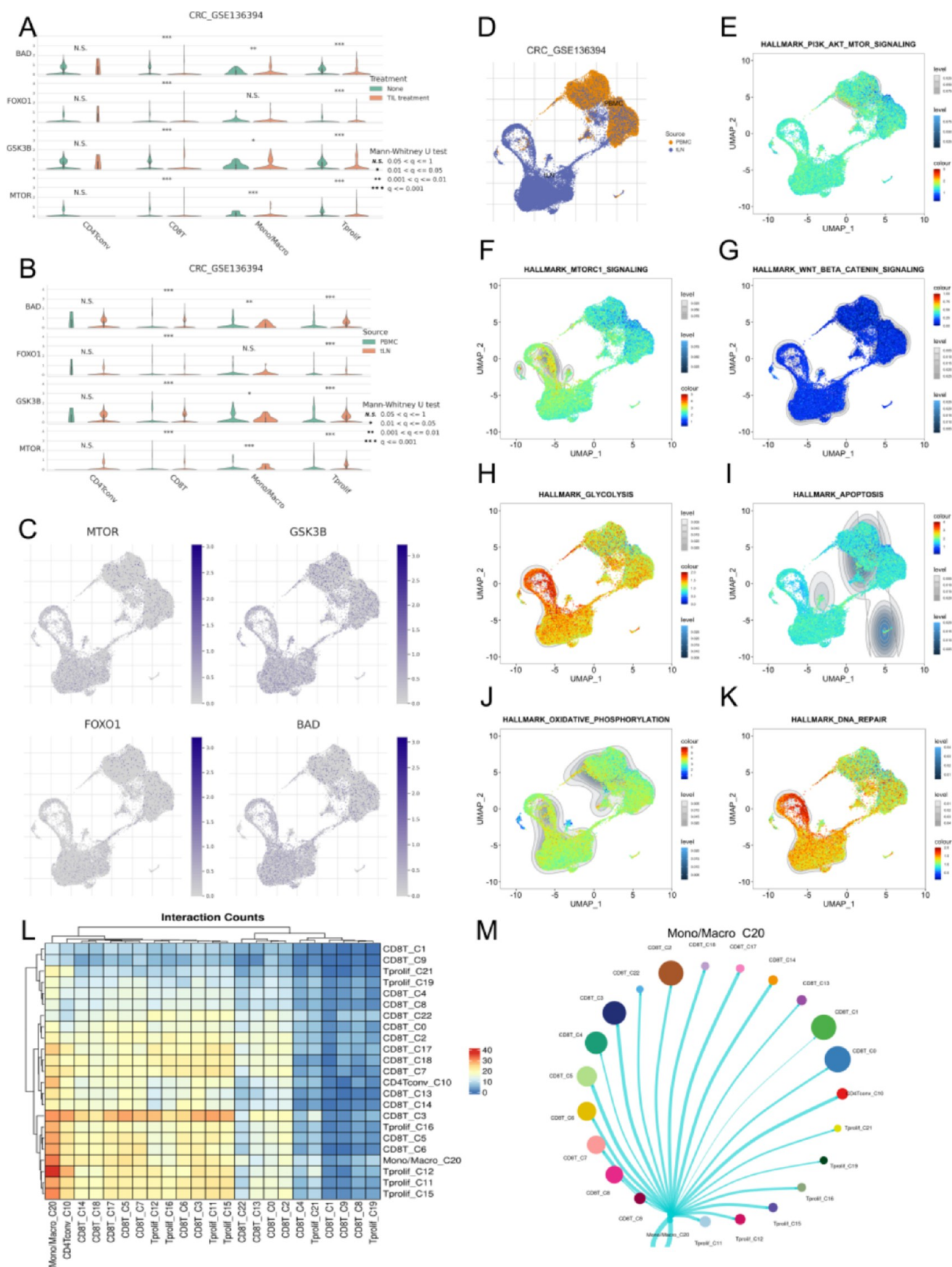


Figure 13. Single-cell transcriptomic analysis of AKT1 activation and its downstream regulatory targets. (A) Immunotherapy analysis about BAD, FOXO1, GSK3B and MTOR. (B) Differential Expression of BAD, FOXO1, GSK3B, and MTOR between PMBC and tLN. (C) AKT1, TP53, PTGS2 and VEGFA gene expression in PMBC and tLN. (D–K) UMAP plot of HALLMARK gene set expression. (L, M) Cell–cell Communication Analysis.

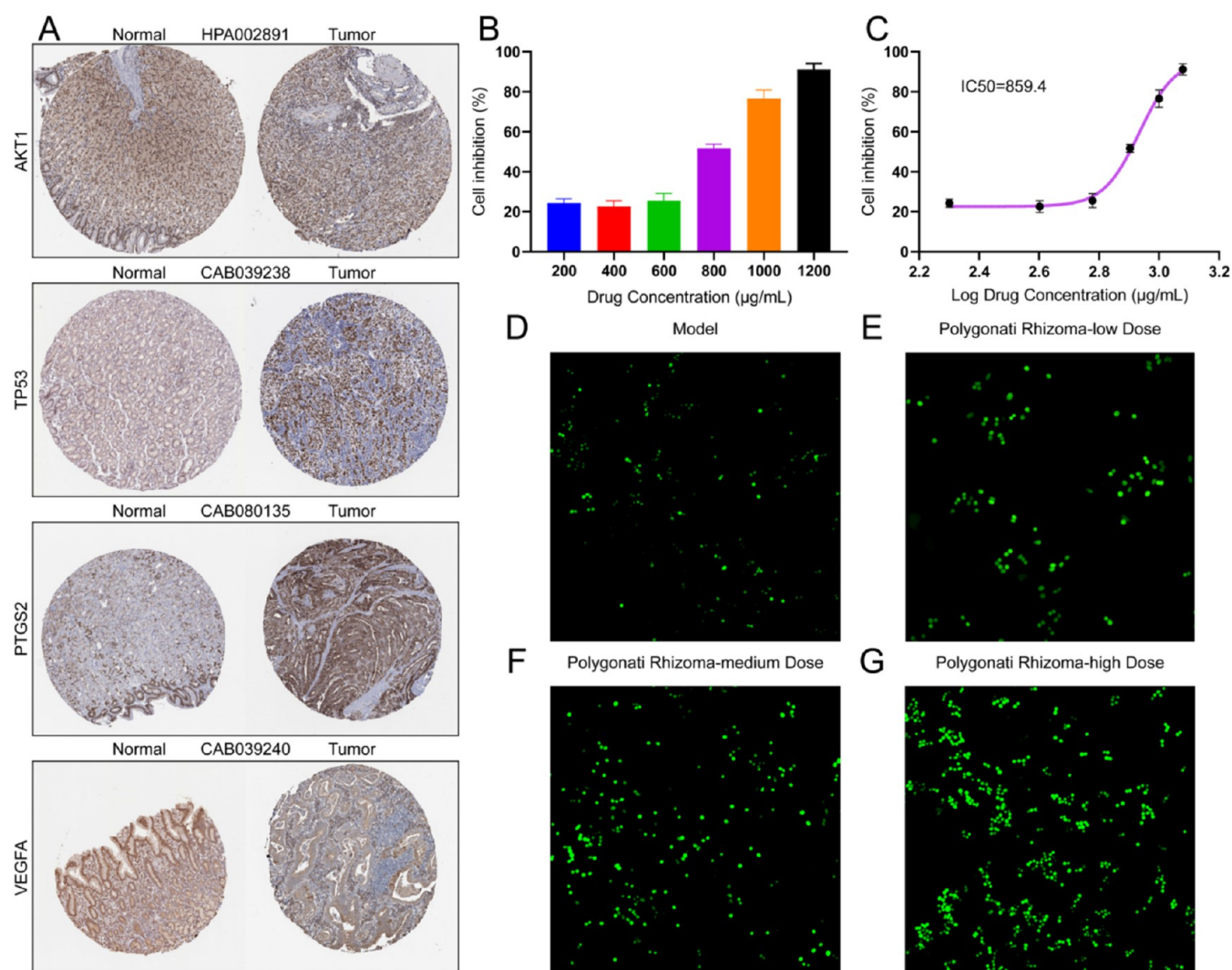


Figure 14. Experimental Validation. (A) Immunohistochemical staining images from the HPA database. (B–C) CCK8 assay. (D–G) Reactive oxygen species (ROS) detection.

3.9. Single-Cell Analysis of Common Digestive System Tumors in Immunotherapy. In CHOL, immunotherapy analysis was performed using the GSE125449 data set. Through cell annotation and clustering, 18 distinct cell types were identified, with the highest proportion of cells classified as hepatic progenitors (Figure 10A–C). The expression patterns of key genes—AKT1, PTGS2, TP53, and VEGFA—across various cell types in the CHOL_GSE125449_aPD1aPDL1aCTLA4 data set revealed distinct cell-type-specific transcriptional activities (Figure 10D–G).

AKT1 exhibited relatively uniform expression across all cell types, with slightly elevated levels in hepatic progenitor and malignant cells, suggesting its broad involvement in cellular signaling pathways within the tumor microenvironment. PTGS2, on the other hand, showed minimal expression in most cell types but displayed a marked increase in malignant cells, emphasizing its potential role in the inflammatory processes and tumor progression associated with malignancy. Notably, TP53 expression was predominantly enriched in malignant cells, consistent with its critical role as a tumor suppressor and its involvement in maintaining genomic stability. VEGFA, a key pro-angiogenic factor, demonstrated the highest expression in malignant and hepatic progenitor cells, under-

scoring its pivotal contribution to angiogenesis and tumor vascularization. The differential expression of these key genes emphasizes their potential roles in shaping the tumor microenvironment, particularly within the malignant and hepatic progenitor cell populations.

Following immunotherapy, significant expression differences of AKT1, PTGS2, TP53, and VEGFA were observed between the treatment and nontreatment groups (Figure 10H). Cell communication analysis further revealed that hepatic progenitor cells were strongly associated with various other cell types, illustrating the dynamic interactions between cell populations within the tumor microenvironment (Figure 10I–M).

3.9.1. Single-Cell Analysis of LIHC in Immunotherapy. In LIHC, immunotherapy analysis was conducted using the GSE125449 data set. Through cell annotation and clustering, 14 distinct cell types were identified, with the highest proportion of cells classified as malignant (Figures 11A–C). Similar to the findings in CHOL, we observed that AKT1, PTGS2, TP53, and VEGFA were widely distributed across various cell types, with VEGFA being particularly enriched in malignant cells (Figures 11D–G).

Following immunotherapy, VEGFA was significantly upregulated in fibroblasts in the treatment group compared to the

nontreatment group. Additionally, AKT1, TP53, and VEGFA were significantly upregulated in hepatic progenitor cells, while AKT1 and VEGFA were significantly upregulated in malignant cells. VEGFA was also significantly upregulated in Mono/Macro cells (Figure 11H). These findings suggest that immunotherapy influences the expression of key genes in different cell populations within the tumor microenvironment, with VEGFA playing a prominent role in immune modulation and tumor progression.

3.9.2. Single-Cell Analysis of CRC in Immunotherapy. In CRC, we conducted an immunotherapy analysis using the data set GSE179784. Through cell annotation and clustering, 12 distinct cell types were identified, with the highest proportion of cells classified as epithelial (Figures 12A–C). Consistent with previous findings, AKT1, PTGS2, TP53, and VEGFA were found to be distributed across various cell types, with VEGFA being particularly enriched in epithelial cells (Figures 12D–G).

In another data set, GSE136394, after immunotherapy, we observed that in the TIL treatment group of CD8+ T cells, the expression of these four genes (AKT1, PTGS2, TP53, and VEGFA) was significantly upregulated compared to the nontreatment group. Additionally, AKT1 and TP53 also exhibited significant expression changes in Tprolif cells before and after immunotherapy (Figure 12H–K). These results suggest that immunotherapy enhances the expression of key genes in specific immune cell populations, highlighting their potential role in modulating the tumor microenvironment and immune response in CRC.

To further determine the activation status of AKT1, we analyzed the expression levels of its key downstream target genes and the associated pathway activities. Following Tumor-Infiltrating Lymphocyte (TIL) treatment, the AKT1-regulated genes BAD, FOXO1, GSK3B, and MTOR were significantly upregulated in CD8 T cells and T proliferating cells. Additionally, BAD, GSK3B, and MTOR were markedly elevated in monocytes/macrophages (Mono/Macro) (Figure 13A). These genes were found to be broadly distributed across both peripheral blood mononuclear cell (PBMC) and Tumor-draining Lymph Nodes (tLN) (Figures 13C,D). Notably, their expression levels were significantly higher in PBMCs compared to tLNs, suggesting systemic activation of the AKT1 pathway, whereas the reduced expression in tLNs may reflect the presence of a tumor-associated immunosuppressive microenvironment (Figure 13B).

Pathway enrichment analysis of these downstream genes was conducted using HALLMARK gene sets as a reference. We observed significant enrichment of PI3K_AKT_MTOR_SIGNALING, MTORC1_SIGNALING, GLYCOLYSIS, APOPTOSIS, OXIDATIVE_PHOSPHORYLATION, and DNA_REPAIR pathways, with GLYCOLYSIS and DNA_REPAIR notably enriched in both PBMCs and tLNs (Figure 13E–K). These findings collectively indicate an activated state of the AKT1 signaling axis.

Furthermore, cell–cell communication analysis revealed that Mono/Macro cells exhibited extensive interactions with multiple immune cell populations (Figures 13L,M), implying that AKT1 activation may modulate the tumor immune response by orchestrating monocyte/macrophage-mediated intercellular signaling with other immune subsets.

In summary, the single-cell analysis revealed cell type-specific expression patterns of AKT1, PTGS2, TP53, and VEGFA in digestive system tumors such as CHOL, LIHC, and CRC, as well as their dynamic changes before and after immunotherapy.

These findings underscore the crucial roles of these key genes in tumor microenvironment remodeling and immune therapy response. Notably, the significant upregulation of VEGFA is closely associated with tumor angiogenesis, while the expression changes of AKT1 and TP53 in CD8+ T and proliferative T cells suggest their potential involvement in the mechanisms underlying immunotherapy efficacy. This study provides valuable theoretical support for exploring new therapeutic targets and optimizing immunotherapy strategies, offering a strong foundation for the advancement of precision medicine.

3.10. Experimental Validation. First, the expression differences of AKT1, TP53, PTGS2, and VEGFA between normal and tumor tissues were analyzed using immunohistochemical staining results from the HPA database (Figure 14A). The analysis revealed that the staining intensity of AKT1 was significantly higher in tumor tissues compared to normal tissues, suggesting that AKT1 is more actively expressed in tumor cells and may be involved in signal transduction and the regulation of cell proliferation in cancer. TP53 showed notably higher expression in tumor tissues, with a widespread distribution, consistent with its role as a tumor suppressor in regulating genomic stability and the cell cycle. PTGS2 expression was significantly enhanced in tumor tissues, indicating its potential involvement in tumor-associated inflammation and progression. VEGFA expression was markedly higher in tumor tissues, particularly in areas with dense blood vessels, reinforcing its critical role in tumor angiogenesis and the remodeling of the tumor microenvironment. These findings suggest that all four genes are overexpressed in tumor tissues and may collectively contribute to tumorigenesis, development, and immune therapy mechanisms.

The CCK8 assay results demonstrated that Polygonati Rhizoma significantly inhibited the proliferation of the gastric cancer cell line HGC-27 in a concentration-dependent manner (Figure 14B,C). As the concentration of the extract increased from 200 $\mu\text{g/mL}$ to 1200 $\mu\text{g/mL}$, the cell inhibition rate progressively increased, with an IC₅₀ value of 859.4 $\mu\text{g/mL}$. Based on these results, 600, 800, and 1000 $\mu\text{g/mL}$ were selected as the low, medium, and high-dose groups for further evaluation, with a model group for comparison.

To evaluate the impact of Polygonati Rhizoma on oxidative stress in gastric cancer cells, we measured the intracellular reactive oxygen species (ROS) levels after treatment with different doses of Polygonati Rhizoma (Figure 14D–G). In the model group, ROS fluorescence signals were weak, indicating a low baseline oxidative stress level (Figure 14D). In the low-dose Polygonati Rhizoma group (600 $\mu\text{g/mL}$), the fluorescence signal slightly increased (Figure 14E), while the medium-dose (800 $\mu\text{g/mL}$) and high-dose (1000 $\mu\text{g/mL}$) groups showed significantly stronger fluorescence signals (Figure 14F,G), demonstrating a dose-dependent enhancement. Elevated ROS levels play a dual role in cancer biology; while moderate ROS levels promote tumor progression, excessive ROS accumulation can trigger oxidative damage, leading to apoptosis or growth inhibition. Our findings suggest that Polygonati Rhizoma significantly increases ROS levels in gastric cancer cells, potentially disrupting redox homeostasis and inducing oxidative stress-mediated apoptosis. This aligns with previous reports that highlight ROS as a key mediator of chemotherapy-induced cytotoxicity in cancer cells. These results suggest that Polygonati Rhizoma can elevate ROS levels in gastric cancer cells, which may induce apoptosis or inhibit cell proliferation by

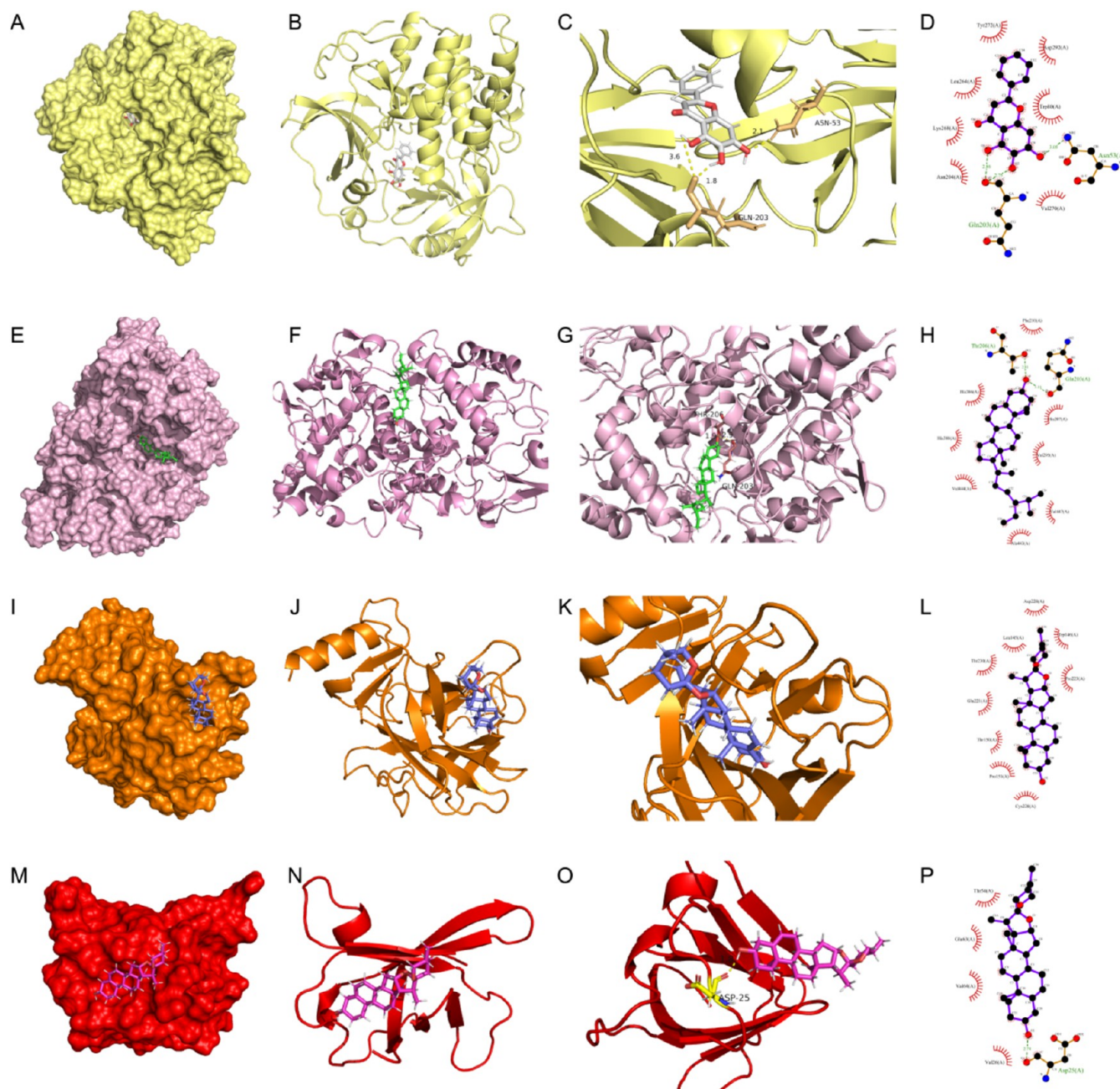


Figure 15. Binding mode of the protein–ligand complex at the equilibrium state of molecular dynamics simulation. (A–D) AKT1–baicalein; (E–H) PTGS2– β -sitosterol; (I–L) TP53–diosgenin; (M–P) VEGFA–diosgenin.

promoting oxidative stress, providing new evidence for its antitumor mechanisms.

3.11. Molecular Simulation and Activity Prediction of Polygonati Rhizoma for Targeted Therapy Based on Computational Chemistry and Physical Modeling. To further validate whether Polygonati Rhizoma exerts its effects by directly targeting AKT1, TP53, PTGS2, and VEGFA and modulating their associated oncogenic signaling pathways, a series of computational simulations were performed. These included MD simulations, RMSD, RMSF, binding free energy calculations, and biological activity (K_i) prediction. These approaches enabled the assessment of binding stability between active compounds and target proteins at the molecular level and provided insights into their potential interaction modes, thereby offering theoretical support for their regulatory mechanisms.

Based on the prior molecular docking results, we selected the following representative protein–ligand complexes for MD simulation: AKT1–baicalein, PTGS2– β -sitosterol, TP53–diosgenin, and VEGFA–diosgenin. Upon reaching equilibrium during the simulations, all active compounds from Polygonati Rhizoma were observed to stably bind within the active binding sites of their respective target proteins. The interactions were primarily stabilized by hydrogen bonds and hydrophobic interactions between the ligands and the key active site residues of AKT1, TP53, PTGS2, and VEGFA. These strong and stable interactions further support the hypothesis that Polygonati Rhizoma possesses the potential to target these proteins and interfere with their oncogenic signaling cascades (Figures 15A–P).

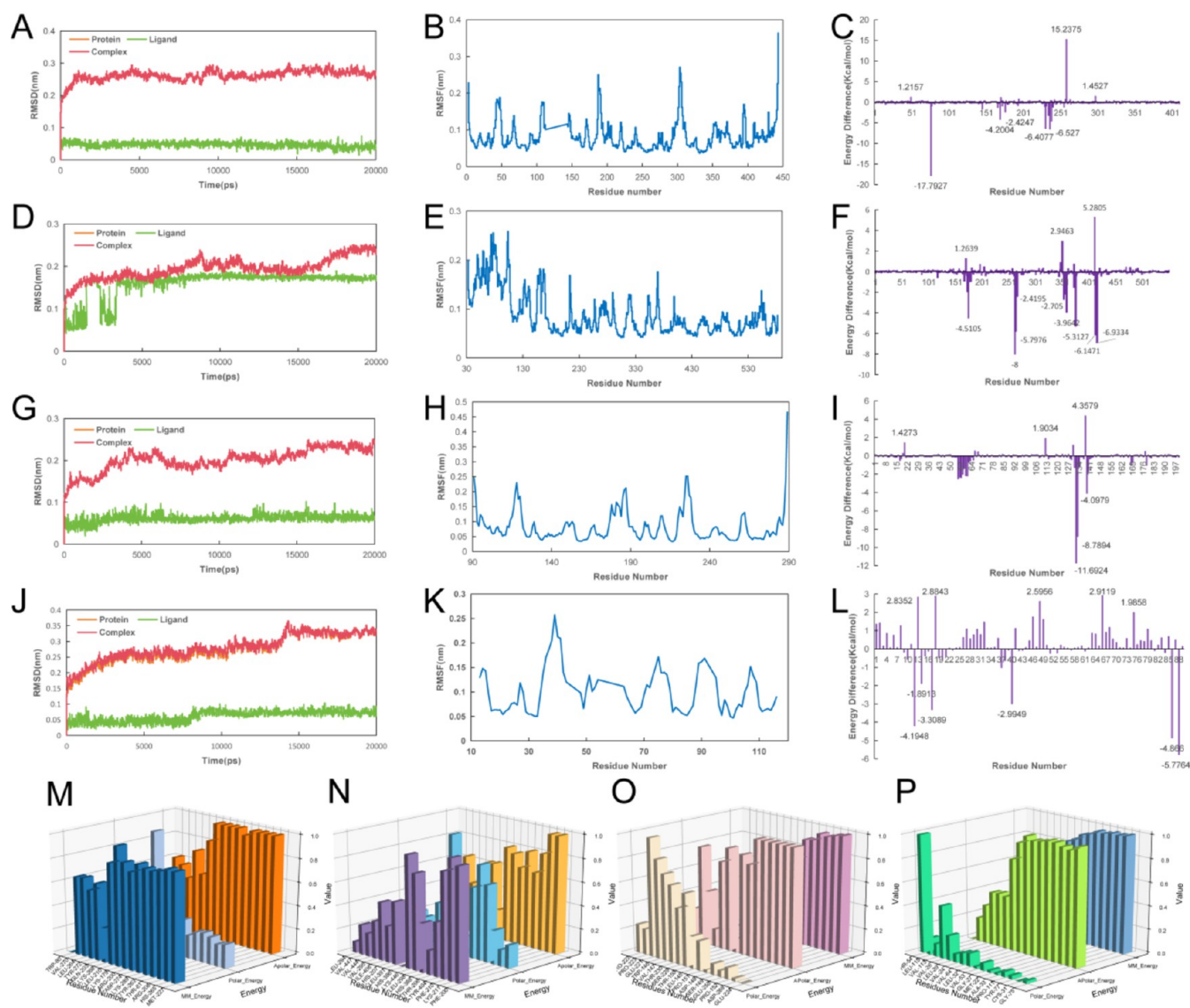


Figure 16. RMSD, RMSF and energy decomposition and distribution of amino acid residues during MD simulation. (A–C, M) AKT1–baicalein; (D–F, N) PTGS2– β -sitosterol; (G–I, O) TP53–diosgenin; (J–L, P) VEGFA–diosgenin.

Table 2. Contributions of Various Energy Components to the Binding Free Energy (kJ/mol) and the Predicted Bioactivities of the Compounds

complexes	ΔE_{vdw}	$\Delta E_{electrostatic}$	$\Delta G_{PB/GB}$	ΔG_{SA}	ΔG_{bind}	K_i (μM)
AKT1-baicalein	−155.655	−32.655	108.745	−15.222	−94.787	3.82×10^{-17}
PTGS2- β -sitosterol	−207.976	−13.987	81.684	−23.560	−164.006	1.51×10^{-29}
TP53-diosgenin	−178.002	−5.293	66.969	−16.331	−132.434	2.07×10^{-24}
VEGFA-diosgenin	−91.836	−8.576	83.972	−11.787	−28.150	1.12×10^{-05}

The RMSD curves demonstrated that during the 20,000 ps molecular dynamics simulation, the protein, ligand, and protein–ligand complexes reached equilibrium after an initial period of fluctuation, indicating stable conformations over time (Figure 16A,D,G,J). The RMSF profiles revealed the structural flexibility of the protein residues upon binding with the four active small-molecule ligands from Polygonati Rhizoma (Figure 16B,E,H,K). Overall, the core regions of the target proteins remained relatively stable, with larger fluctuations observed at the terminal ends or specific residue sites, all within an acceptable range.

Figure 16C,F,I,L show the per-residue energy decomposition profiles of key amino acids within the active binding sites of the protein–ligand complexes. These residues were found to be critical for maintaining the structural stability of the complexes, supporting the notion that AKT1, TP53, PTGS2, and VEGFA interact with the Polygonati Rhizoma-derived ligands through multiple essential active site residues.

Furthermore, Figure 16M–P highlight the top six residues contributing most significantly to the stability of each complex. Notably, the energy distribution among residues such as Gln203, Asn53, Thr206, and Asp25 confirmed that hydrogen bonding interactions involving these sites played a key role in the

formation and stabilization of the protein–ligand systems. These findings strengthen the reliability of both molecular docking and MD simulations, further supporting the hypothesis that AKT1, TP53, PTGS2, and VEGFA serve as effective targets of Polygonati Rhizoma active compounds.

To evaluate the bioactivity of the chemical constituents in Polygonati Rhizoma and to estimate the binding free energies between the active compounds and their predicted targets, the MM-PBSA method was employed. Table 2 presents the detailed energetic contributions, including van der Waals energy (ΔE_{vdw}), electrostatic energy ($\Delta E_{\text{electrostatic}}$), as well as polar and nonpolar solvation energies.

The results revealed that all four active compounds exhibited remarkably low binding free energies (ranging from -28.150 to -164.006 kJ/mol) and low predicted K_i values, indicating strong binding affinities toward their respective targets. Notably, for all compound–target interactions, ΔE_{vdw} was consistently lower than $\Delta E_{\text{electrostatic}}$, suggesting that van der Waals interactions play a dominant role in stabilizing the ligand–target complexes.

In addition, the decomposition of binding energy components indicated that nonpolar solvation energy (ΔG_{SA}) contributed more favorably to the total binding free energy compared to polar solvation energy, further emphasizing the importance of hydrophobic interactions. Taken together, these findings suggest that ΔE_{vdw} and polar solvation energy are the primary contributors to the binding free energy.

Overall, the MM-PBSA results provide compelling evidence that Polygonati Rhizoma exhibits high binding affinity and potential bioactivity against the targets AKT1, TP53, PTGS2, and VEGFA, supporting its therapeutic relevance in modulating oncogenic signaling pathways.

4. DISCUSSION

Stomach adenocarcinoma (STAD) is one of the most common and aggressive malignancies in the digestive system, characterized by poor prognosis and high metastatic potential.⁵² Despite advances in conventional therapies, the treatment of STAD remains challenging, and new therapeutic strategies are urgently needed.⁵³ Polygonati Rhizoma, the rhizome of Polygonatum species, is a traditional Chinese medicinal herb known for its immune-modulatory, anti-inflammatory, and anticancer properties.⁵⁴ Previous studies have demonstrated its potential in enhancing immune function and inhibiting tumor growth, making it a promising candidate for complementary cancer treatment.⁵⁵ In this study, we utilized advanced artificial intelligence (AI) techniques, including bioinformatics methods, machine learning (ML), network pharmacology, and single-cell RNA sequencing, to explore the immunomodulatory mechanisms of Polygonati Rhizoma in the context of STAD and other digestive system tumors. By leveraging AI-driven analysis, we gained novel insights into how this traditional Chinese medicinal herb could influence tumor immunity, highlighting its potential as a complementary agent in precision oncology.

Our findings demonstrated that key bioactive compounds from Polygonati Rhizoma—such as diosgenin, baicalein, and β -sitosterol—target multiple cancer-related and immune-regulatory pathways. Diosgenin, in particular, exhibited the strongest binding affinity with critical targets like TP53, AKT1, VEGFA, and PTGS2, as confirmed by molecular docking and molecular dynamics simulations. Moreover, considering the chemical characteristics and current research status of Polygonati Rhizoma, its primary active constituents—including saponins,

polysaccharides, and flavonoids—possess complex chemical structures, low water solubility, and, in some cases, limited stability under in vitro experimental conditions. Therefore, we employed a bioactivity prediction method to further verify the feasibility and potential of Polygonati Rhizoma in targeting AKT1, TP53, PTGS2, and VEGFA. The results demonstrated that these genes exhibit strong binding affinities with diosgenin, baicalein, and β -sitosterol, and the resulting biomolecular complexes showed notable bioactivity, supporting the therapeutic relevance of these interactions. Using AI-powered docking simulations, we accurately predicted these binding interactions, providing more reliable evidence of diosgenin's anticancer and immunomodulatory properties, including its role in promoting apoptosis and modulating immune cell activity.^{56,57} Furthermore, baicalein and β -sitosterol have been extensively studied for their anti-inflammatory and antioxidative effects, which may also contribute to enhanced immune surveillance and reduced tumor progression.^{58,59}

One of the most significant contributions of this study is the integration of AI-driven approaches to identify a subset of genes (AKT1, PTGS2, TP53, VEGFA) that not only play pivotal roles in tumor biology but are also highly relevant to the immune microenvironment. AI-based algorithms were utilized to process large-scale genomic data, allowing us to pinpoint these critical genes more efficiently than traditional methods. TP53, a well-known tumor suppressor frequently altered in gastric cancer, has been shown to regulate immune checkpoints and modulate the expression of pro- and anti-inflammatory cytokines.⁶⁰ Consistent with our data, other studies have found that TP53 mutations are associated with altered tumor-infiltrating lymphocyte profiles and worse clinical outcomes in STAD.^{61,62} Similarly, AKT1's involvement in immune evasion and tumor metabolism has been well-documented. Its upregulation in the tumor microenvironment is thought to suppress T-cell activation while promoting the recruitment of regulatory immune cells.^{63,64} Interestingly, PTGS2 (COX-2), a pro-inflammatory enzyme often overexpressed in gastrointestinal cancers, was positively correlated with macrophage and neutrophil infiltration in our analysis. This supports earlier findings that high COX-2 expression creates a pro-inflammatory tumor microenvironment conducive to tumor growth and immune suppression.^{65,66} Therapeutic inhibition of COX-2 has been shown to improve immune responses and sensitize tumors to immune checkpoint blockade, further underscoring its importance as a target.^{67,68}

VEGFA, a key regulator of angiogenesis, was found to be significantly expressed in tumor tissues and correlated with myeloid-derived suppressor cell (MDSC) infiltration. Using AI-driven analysis, we confirmed that VEGFA not only drives tumor vascularization but also contributes to an immunosuppressive microenvironment by recruiting MDSCs and promoting the differentiation of regulatory T cells.^{69,70} Our results support these findings and suggest that targeting VEGFA might improve immune infiltration and enhance the efficacy of immunotherapies in STAD and other digestive system tumors.

Comparing our data with prior studies, we observed that the identified core genes exhibit distinct expression patterns across different cancer types, as shown in the single-cell analyses. For instance, TP53 and PTGS2 were primarily expressed in malignant cells, while VEGFA expression was enriched in both malignant and progenitor-like cells, consistent with its role in tumor maintenance and angiogenesis.^{71,72} By integrating AI-powered single-cell analysis, we were able to gain a more

granular understanding of how Polygonati Rhizoma's active compounds might exert their effects through multiple cellular compartments within the tumor microenvironment. This insight can help improve the efficacy of combination therapies that include immunomodulators or checkpoint inhibitors, making them more personalized.

Our study also explored the prognostic significance of these genes. High expression levels of PTGS2, AKT1, and VEGFA were associated with poor survival outcomes, corroborating earlier reports linking these genes to aggressive tumor behavior and immune evasion.^{73,74} The integration of AI techniques, such as network pharmacology and single-cell transcriptomics, allowed us to pinpoint these critical genes and pathways more efficiently. These AI-driven approaches offer a clearer understanding of how traditional Chinese medicinal components like Polygonati Rhizoma might enhance antitumor immunity and could serve as valuable tools in optimizing cancer treatment strategies.

Nevertheless, this study has certain limitations. Although scRNA-seq data were utilized to analyze gene expression across different cell types, integrative multiomics approaches were not employed to provide a more comprehensive understanding of the immunoregulatory mechanisms involved. Future studies could incorporate genomics, epigenomics, proteomics, and metabolomics, using techniques such as genome-wide association studies (GWAS), ATAC-seq, protein–protein interaction (PPI) network analysis, and metabolic pathway profiling to systematically elucidate the regulatory effects of Polygonati Rhizoma on the immune microenvironment. However, the integration of multiomics data still faces several challenges, including data standardization, computational resource demands, and validation of causal relationships. These issues necessitate further algorithmic optimization and experimental validation to enhance the depth, accuracy, and reliability of future investigations.

5. CONCLUSIONS

In summary, our findings provide valuable insights into the complex interactions between the bioactive compounds of Polygonati Rhizoma and the tumor immune microenvironment. The identified core targets and pathways offer a strong foundation for future studies focused on optimizing these compounds for immunotherapeutic applications. The integration of AI-driven techniques, single-cell analysis, and network pharmacology has proven to be a powerful strategy, enabling a deeper understanding of how these traditional Chinese medicinal compounds influence tumor immunity. Future research should include functional experiments in vivo and clinical trials to validate the therapeutic potential of Polygonati Rhizoma in combination with current immunotherapies. These advancements pave the way for more personalized and effective cancer treatment paradigms, offering new avenues for enhancing the efficacy of immunotherapies in digestive system tumors and beyond.

■ ASSOCIATED CONTENT

SI Supporting Information

The Supporting Information is available free of charge at <https://pubs.acs.org/doi/10.1021/acsomega.5c00981>.

The Supporting Information includes Tables S1 and S2. Table S1: The compounds calculated by ADME model in

the study. Table S2: Effective target calculated by SysDT in the study (PDF)

■ AUTHOR INFORMATION

Corresponding Authors

Yinfeng Yang — School of Medical Informatics Engineering, Anhui University of Chinese Medicine, Hefei, Anhui 230038, China; Anhui Provincial Key Laboratory of Chinese Medicinal Formula, Anhui University of Chinese Medicine, Hefei 230038, China; orcid.org/0000-0002-2557-4807; Email: yinfengyang@yeah.net

Jinghui Wang — School of Integrated Chinese and Western Medicine, Anhui University of Chinese Medicine, Hefei, Anhui 230038, China; Anhui Provincial Key Laboratory of Chinese Medicinal Formula, Anhui University of Chinese Medicine, Hefei 230038, China; orcid.org/0000-0002-8462-3322; Email: jhwang_dlut@163.com

Authors

Peizheng Yang — School of Integrated Chinese and Western Medicine, Anhui University of Chinese Medicine, Hefei, Anhui 230038, China; Anhui Provincial Key Laboratory of Chinese Medicinal Formula, Anhui University of Chinese Medicine, Hefei 230038, China

Xiangyu Wang — School of Integrated Chinese and Western Medicine, Anhui University of Chinese Medicine, Hefei, Anhui 230038, China; Anhui Provincial Key Laboratory of Chinese Medicinal Formula, Anhui University of Chinese Medicine, Hefei 230038, China

Jianhua Yang — School of Medical Informatics Engineering, Anhui University of Chinese Medicine, Hefei, Anhui 230038, China; Anhui Provincial Key Laboratory of Chinese Medicinal Formula, Anhui University of Chinese Medicine, Hefei 230038, China

Biaobiao Yan — School of Integrated Chinese and Western Medicine, Anhui University of Chinese Medicine, Hefei, Anhui 230038, China; Anhui Provincial Key Laboratory of Chinese Medicinal Formula, Anhui University of Chinese Medicine, Hefei 230038, China

Haiyang Sheng — Global Biometrics and Data Sciences, Bristol Myers Squibb, Lawrenceville, New Jersey 10154, United States

Yan Li — Key Laboratory of Industrial Ecology and Environmental Engineering (MOE), Department of Materials Sciences and Chemical Engineering, Dalian University of Technology, Dalian, Liaoning 116023, China; orcid.org/0000-0001-8295-530X

Complete contact information is available at:

<https://pubs.acs.org/10.1021/acsomega.5c00981>

Author Contributions

#P.Y., X.W., and J.Y. are equal contribution to the work.

Notes

The authors declare no competing financial interest.

■ ACKNOWLEDGMENTS

Thanks for the Outstanding Youth Research Project of Anhui, Department of Education (Grant No. 2022AH020042), the Major Scientific Research Project of Universities in Anhui province (Grant No. 2024AH040146), the Anhui Province Quality Projects (Grant No. 2023sdx027) and the Training Action Project of Anhui Provincial Education Department of Young and Middle-aged Teachers (JNFX2023020).

REFERENCES

- (1) Bray, F.; Ferlay, J.; Soerjomataram, I.; Siegel, R. L.; Torre, L. A.; Jemal, A. Global cancer statistics 2018: GLOBOCAN estimates of incidence and mortality worldwide for 36 cancers in 185 countries. *CA-Cancer J. Clin.* **2018**, *68* (6), 394–424.
- (2) Ajani, J. A.; D'Amico, T. A.; Brentem, D. J.; Chao, J.; Cooke, D.; Corvera, C.; Pluchino, L. A.; et al. Gastric cancer, version 2.2022, NCCN clinical practice guidelines in oncology. *J. Natl. Compr. Cancer Network* **2022**, *20* (2), 167–192.
- (3) Smyth, E. C.; Nilsson, M.; Grabsch, H. I.; van Grieken, N. C.; Lordick, F. Gastric cancer. *Lancet* **2020**, *396* (10251), 635–648.
- (4) Chabner, B. A.; Roberts, T. G., Jr. Chemotherapy and the war on cancer. *Nat. Rev. Cancer* **2005**, *5* (1), 65–72.
- (5) Bang, Y. J.; Van Cutsem, E.; Feyereislova, A.; Chung, H. C.; Shen, L.; Sawaki, A.; Kang, Y. K.; et al. Trastuzumab in combination with chemotherapy versus chemotherapy alone for treatment of HER2-positive advanced gastric or gastro-oesophageal junction cancer (ToGA): a phase 3, open-label, randomised controlled trial. *Lancet* **2010**, *376* (9742), 687–697.
- (6) Chung, H. C.; Kang, Y. K.; Chen, Z.; Bai, Y.; Wan Ishak, W. Z.; Shim, B. Y.; Qin, S. K.; et al. Pembrolizumab versus paclitaxel for previously treated advanced gastric or gastroesophageal junction cancer (KEYNOTE-063): a randomized, open-label, phase 3 trial in Asian patients. *Cancer* **2022**, *128* (5), 995–1003.
- (7) Fuchs, C. S.; Doi, T.; Jang, R. W.; Muro, K.; Satoh, T.; Machado, M.; Yoon, H. H. Safety and efficacy of pembrolizumab monotherapy in patients with previously treated advanced gastric and gastroesophageal junction cancer: phase 2 clinical KEYNOTE-059 trial. *JAMA Oncol.* **2018**, *4* (5), e180013.
- (8) Sharma, P.; Allison, J. P. Immune checkpoint targeting in cancer therapy: toward combination strategies with curative potential. *Cell* **2015**, *161* (2), 205–214.
- (9) Postow, M. A.; Callahan, M. K.; Wolchok, J. D. Immune checkpoint blockade in cancer therapy. *J. Clin. Oncol.* **2015**, *33* (17), 1974–1982.
- (10) Hanahan, D.; Weinberg, R. A. Hallmarks of cancer: the next generation. *Cell* **2011**, *144* (5), 646–674.
- (11) Chen, D. S.; Mellman, I. Elements of cancer immunity and the cancer-immune set point. *Nature* **2017**, *541* (7637), 321–330.
- (12) Xiang, Y.; Guo, Z.; Zhu, P.; Chen, J.; Huang, Y. Traditional Chinese medicine as a cancer treatment: Modern perspectives of ancient but advanced science. *Cancer Med.* **2019**, *8* (5), 1958–1975.
- (13) Fu, K.; Hui, B.; Wang, Q.; Lu, C.; Shi, W.; Zhang, Z.; Chen, Z.; et al. Single-cell RNA sequencing of immune cells in gastric cancer patients. *Aging* **2020**, *12* (3), 2747.
- (14) Zhao, L.; Xu, C.; Zhou, W.; Li, Y.; Xie, Y.; Hu, H.; Wang, Z. Polygonati Rhizoma with the homology of medicine and food: A review of ethnopharmacology, botany, phytochemistry, pharmacology and applications. *J. Ethnopharmacol.* **2023**, *309*, No. 116296.
- (15) Yang, G.; Jiang, D.; Chen, B.; Huang, J.; Huang, L. J.; Li, N. Biochemical compounds and pharmacological functions of a traditional Chinese medicinal herb Polygonati rhizoma. *Medicinal Plant Biology* **2024**, *3* (1), e012 DOI: 10.48130/mpb-0024-0009.
- (16) Xu, C.; Xia, B.; Zhang, Z.; Lin, Y.; Li, C.; Lin, L. Research progress in steroidal saponins from the genus Polygonatum: chemical components, biosynthetic pathways and pharmacological effects. *Phytochemistry* **2023**, *213*, No. 113731.
- (17) Hopkins, A. L. Network pharmacology: the next paradigm in drug discovery. *Nat. Chem. Biol.* **2008**, *4* (11), 682–690.
- (18) Huang, D. W.; Sherman, B. T.; Lempicki, R. A. Systematic and integrative analysis of large gene lists using DAVID bioinformatics resources. *Nat. Protoc.* **2009**, *4* (1), 44–57.
- (19) He, Y.; Huang, L.; Jiang, P.; Xu, G.; Sun, T. Immunological regulation of the active fraction from Polygonatum sibiricum F. Delaroche based on improvement of intestinal microflora and activation of RAW264. 7 cells. *J. Ethnopharmacol.* **2022**, *293*, No. 115240.
- (20) Zhang, J.; Wang, Y. Z.; Yang, M. Q.; Yang, W. Z.; Yang, S. B.; Zhang, J. Y. Identification and evaluation of Polygonatum kingianum with different growth ages based on data fusion strategy. *Microchem. J.* **2021**, *160*, No. 105662.
- (21) Luo, S.; Zhang, X.; Huang, S.; Feng, X.; Zhang, X.; Xiang, D. A monomeric polysaccharide from Polygonatum sibiricum improves cognitive functions in a model of Alzheimer's disease by reshaping the gut microbiota. *Int. J. Biol. Macromol.* **2022**, *213*, 404–415.
- (22) Zhao, L.; Zhang, H.; Li, N.; Chen, J.; Xu, H.; Wang, Y.; Liang, Q. Network pharmacology, a promising approach to reveal the pharmacology mechanism of Chinese medicine formula. *J. Ethnopharmacol.* **2023**, *309*, No. 116306.
- (23) Kumar, V.; Ramnarayanan, K.; Sundar, R.; Padmanabhan, N.; Srivastava, S.; Koiwa, M.; Tan, P.; et al. Single-cell atlas of lineage states, tumor microenvironment, and subtype-specific expression programs in gastric cancer. *Cancer Discovery* **2022**, *12* (3), 670–691.
- (24) Xu, J.; Yu, B.; Wang, F.; Yang, J. Single-cell RNA sequencing to map tumor heterogeneity in gastric carcinogenesis paving roads to individualized therapy. *Cancer Immunol., Immunotherapy* **2024**, *73* (11), 233.
- (25) Ru, J.; Li, P.; Wang, J.; Zhou, W.; Li, B.; Huang, C.; Yang, L.; et al. TCMSP: a database of systems pharmacology for drug discovery from herbal medicines. *J. Cheminf.* **2014**, *6*, 1–6.
- (26) UniProt Consortium, T.. UniProt: the universal protein knowledgebase. *Nucleic Acids Res.* **2018**, *46* (5), 2699.
- (27) Stelzer, G.; Rosen, N.; Plaschkes, I.; Zimmerman, S.; Twik, M.; Fishilevich, S.; Lancet, D.; et al. The GeneCards suite: from gene data mining to disease genome sequence analyses. *Current Protocols Bioinformatics* **2016**, *54* (1), 1–30.
- (28) Xu, X.; Zhang, W.; Huang, C.; Li, Y.; Yu, H.; Wang, Y.; Duan, J.; Ling, Y. A novel chemometric method for the prediction of human oral bioavailability. *Int. J. Molecular Sciences* **2012**, *13* (6), 6964–6982.
- (29) Willett, P.; Barnard, J. M.; Downs, G. M. Chemical similarity searching. *J. Chem. Inf. Comput. Sci.* **1998**, *38* (6), 983–996.
- (30) Wishart, D. S.; Knox, C.; Guo, A. C.; Cheng, D.; Shrivastava, S.; Tzur, D.; Gautam, B.; Hassanali, M. DrugBank: a knowledgebase for drugs, drug actions and drug targets. *Nucleic Acids Res.* **2008**, *36* (suppl_1), D901–D906.
- (31) Yu, H.; Chen, J.; Xu, X.; Li, Y.; Zhao, H.; Fang, Y.; Wang, Y.; et al. A systematic prediction of multiple drug-target interactions from chemical, genomic, and pharmacological data. *PLoS One* **2012**, *7* (5), No. e37608.
- (32) Franz, M.; Lopes, C. T.; Huck, G.; Dong, Y.; Sumer, O.; Bader, G. D. Cytoscape.js: a graph theory library for visualisation and analysis. *Bioinformatics* **2016**, *32* (2), 309–311.
- (33) Shannon, P.; Markiel, A.; Ozier, O.; Baliga, N. S.; Wang, J. T.; Ramage, D.; Ideker, T.; et al. Cytoscape: a software environment for integrated models of biomolecular interaction networks. *Genome Res.* **2003**, *13* (11), 2498–2504.
- (34) Zhou, Y.; Zhou, B.; Pache, L.; Chang, M.; Khodabakhshi, A. H.; Tanaseichuk, O.; Benner, C.; Chanda, S. K. Metascape provides a biologist-oriented resource for the analysis of systems-level datasets. *Nat. Commun.* **2019**, *10* (1), No. 1523.
- (35) Warde-Farley, D.; Donaldson, S. L.; Comes, O.; Zuberi, K.; Badrawi, R.; Chao, P.; Morris, Q.; et al. The GeneMANIA prediction server: biological network integration for gene prioritization and predicting gene function. *Nucleic Acids Res.* **2010**, *38* (suppl_2), W214–W220.
- (36) Sherry, S. T.; Ward, M. H.; Kholodov, M.; Baker, J.; Phan, L.; Smigielski, E. M.; Sirotkin, K. dbSNP: the NCBI database of genetic variation. *Nucleic Acids Res.* **2001**, *29* (1), 308–311.
- (37) Waterhouse, A.; Bertoni, M.; Bienert, S.; Studer, G.; Tauriello, G.; Gumienny, R.; Schwede, T.; et al. SWISS-MODEL: homology modelling of protein structures and complexes. *Nucleic Acids Res.* **2018**, *46* (W1), W296–W303.
- (38) Kim, S.; Thiessen, P. A.; Bolton, E. E.; Chen, J.; Fu, G.; Gindulyte, A.; Bryant, S. H.; et al. PubChem substance and compound databases. *Nucleic Acids Res.* **2016**, *44* (D1), D1202–D1213.
- (39) Schiffrin, B.; Radford, S. E.; Brockwell, D. J.; Calabrese, A. N. PyXlinkViewer: A flexible tool for visualization of protein chemical

crosslinking data within the PyMOL molecular graphics system. *Protein Sci.* **2020**, *29* (8), 1851–1857.

(40) Morris, G. M.; Huey, R.; Lindstrom, W.; Sanner, M. F.; Belew, R. K.; Goodsell, D. S.; Olson, A. J. AutoDock4 and AutoDockTools4: Automated docking with selective receptor flexibility. *J. Comput. Chem.* **2009**, *30* (16), 2785–2791.

(41) Berendsen, H. J.; van der Spoel, D.; van Drunen, R. GROMACS: A message-passing parallel molecular dynamics implementation. *Comput. Phys. Commun.* **1995**, *91* (1–3), 43–56.

(42) Hornak, V.; Abel, R.; Okur, A.; Strockbine, B.; Roitberg, A.; Simmerling, C. Comparison of multiple Amber force fields and development of improved protein backbone parameters. *Proteins* **2006**, *65* (3), 712–725.

(43) Lin, J. H.; Perryman, A. L.; Schames, J. R.; McCammon, J. A. Computational drug design accommodating receptor flexibility: the relaxed complex scheme. *J. Am. Chem. Soc.* **2002**, *124* (20), 5632–5633.

(44) Parrinello, M.; Rahman, A. Polymorphic transitions in single crystals: A new molecular dynamics method. *J. Appl. Phys.* **1981**, *52* (12), 7182–7190.

(45) Kumari, R.; Kumar, R.; Open Source Drug Discovery Consortium; Lynn, A. g_mmpbsa— A GROMACS tool for high-throughput MM-PBSA calculations. *J. Chem. Inf. Model.* **2014**, *54* (7), 1951–1962.

(46) Jedrzejewski, M. J.; Singh, S.; Brouillette, W. J.; Air, G. M.; Luo, M. A strategy for theoretical binding constant, K_i , calculations for neuraminidase aromatic inhibitors designed on the basis of the active site structure of influenza virus neuraminidase. *Proteins* **1995**, *23* (2), 264–277.

(47) Jangam, C. S.; Bhowmick, S.; Chorge, R. D.; Bharatralo, L. D.; Patil, P. C.; Chikhale, R. V.; Islam, M. A.; et al. Pharmacoinformatics-based identification of anti-bacterial catalase-peroxidase enzyme inhibitors. *Computational Biol. Chem.* **2019**, *83*, No. 107136.

(48) Vogelstein, B.; Lane, D.; Levine, A. J. Surfing the p53 network. *Nature* **2000**, *408* (6810), 307–310.

(49) Li, H. B.; Cheng, K. W.; Wong, C. C.; Fan, K. W.; Chen, F.; Jiang, Y. Evaluation of antioxidant capacity and total phenolic content of different fractions of selected microalgae. *Food Chem.* **2007**, *102* (3), 771–776.

(50) Cheung, E. C.; Vousden, K. H. The role of ROS in tumour development and progression. *Nat. Rev. Cancer* **2022**, *22* (5), 280–297.

(51) Yang, H.; Villani, R. M.; Wang, H.; Simpson, M. J.; Roberts, M. S.; Tang, M.; Liang, X. The role of cellular reactive oxygen species in cancer chemotherapy. *J. Experim. Clinical Cancer Res.* **2018**, *37*, 1–10.

(52) Ilic, M.; Ilic, I. Epidemiology of stomach cancer. *World J. Gastroenterol.* **2022**, *28* (12), 1187.

(53) Joshi, S. S.; Badgwell, B. D. Current treatment and recent progress in gastric cancer. *CA-Cancer J. Clin.* **2021**, *71* (3), 264–279.

(54) Yang, G.; Jiang, D.; Chen, B.; Huang, J.; Huang, L. J.; Li, N. Biochemical compounds and pharmacological functions of a traditional Chinese medicinal herb *Polygonati rhizoma*. *Med. Plant Biol.* **2024**, *3* (1), e012 DOI: 10.48130/mpb-0024-0009.

(55) Nkuété, A.; Migliolo, L.; Wabo, H.; Tane, P.; Franco, O. Evaluation of multiple functions of *Polygonum* genus compounds. *European J. Med. Plants* **2015**, *6* (1), 1–16.

(56) Michalak, O.; Krzeczynski, P.; Cieślak, M.; Cmocho, P.; Cybulski, M.; Królewska-Golińska, K.; Ostrowska, K.; et al. Synthesis and anti-tumour, immunomodulating activity of diosgenin and tigogenin conjugates. *J. Steroid Biochem. Mol. Biol.* **2020**, *198*, No. 105573.

(57) Semwal, P.; Painuli, S.; Abu-Izneid, T.; Rauf, A.; Sharma, A.; Daştan, S. D.; Cho, W. C.; et al. Diosgenin: an updated pharmacological review and therapeutic perspectives. *Oxidative Med. Cellular Longevity* **2022**, *2022* (1), No. 1035441.

(58) Rahmani, A. H.; Almatroudi, A.; Khan, A. A.; Babiker, A. Y.; Alanezi, M.; Allemailem, K. S. The multifaceted role of baicalein in cancer management through modulation of cell signalling pathways. *Molecules* **2022**, *27* (22), 8023.

(59) Rashed, K. Beta-sitosterol medicinal properties: A review article. *J. Sci. Innov. Technol.* **2020**, *9*, 208–212.

(60) Jiang, Z.; Liu, Z.; Li, M.; Chen, C.; Wang, X. Immunogenomics analysis reveals that TP53 mutations inhibit tumor immunity in gastric cancer. *Translational Oncol.* **2018**, *11* (5), 1171–1187.

(61) Petitjean, A.; Achatz, M. I. W.; Borresen-Dale, A. L.; Hainaut, P.; Olivier, M. TP53 mutations in human cancers: functional selection and impact on cancer prognosis and outcomes. *Oncogene* **2007**, *26* (15), 2157–2165.

(62) Cui, Y.; Guo, G. Immunomodulatory function of the tumor suppressor p53 in host immune response and the tumor microenvironment. *Int. J. Molecular Sci.* **2016**, *17* (11), 1942 DOI: 10.3390/ijms17111942.

(63) Vara, J. A. F.; Casado, E.; de Castro, J.; Cejas, P.; Belda-Iniesta, C.; González-Barón, M. PI3K/Akt signalling pathway and cancer. *Cancer Treatment Rev.* **2004**, *30* (2), 193–204.

(64) Tufail, M.; Wan, W. D.; Jiang, C.; Li, N. Targeting PI3K/AKT/mTOR Signaling to Overcome Drug Resistance in Cancer. *Chem.-Biol. Interact.* **2024**, *396*, No. 111055.

(65) Wang, D.; DuBois, R. N. Eicosanoids and cancer. *Nat. Rev. Cancer* **2010**, *10* (3), 181–193.

(66) Sansone, P.; Piazza, G.; Paterini, P.; Strillacci, A.; Ceccarelli, C.; Minni, F.; Bonafe, M.; et al. Cyclooxygenase-2/carbonic anhydrase-IX up-regulation promotes invasive potential and hypoxia survival in colorectal cancer cells. *J. Cell. Mol. Med.* **2009**, *13* (9b), 3876–3887.

(67) Shimizu, K.; Okita, R.; Saisho, S.; Maeda, A. I.; Nojima, Y.; Nakata, M. Impact of COX2 inhibitor for regulation of PD-L1 expression in non-small cell lung cancer. *Anticancer Res.* **2018**, *38* (8), 4637–4644.

(68) Rodrigues, P.; Bangali, H.; Hammoud, A.; Mustafa, Y. F.; Al-Hetty, H. R. A. K.; Alkhafaji, A. T.; Alsalamy, A.; et al. COX 2-inhibitors; a thorough and updated survey into combinational therapies in cancers. *Med. Oncol.* **2024**, *41* (1), 41.

(69) Carmeliet, P.; Jain, R. K. Principles and mechanisms of vessel normalization for cancer and other angiogenic diseases. *Nat. Rev. Drug Discovery* **2011**, *10* (6), 417–427.

(70) Li, Y. L.; Zhao, H.; Ren, X. B.; et al. Relationship of VEGF/VEGFR with immune and cancer cells: staggering or forward? *Cancer Biol. Med.* **2016**, *13* (2), 206.

(71) Tabassum, D. P.; Polyak, K. Tumorigenesis: it takes a village. *Nat. Rev. Cancer* **2015**, *15* (8), 473–483.

(72) Geng, Y.; Feng, J.; Huang, H.; Wang, Y.; Yi, X.; Wei, S.; Hu, W.; et al. Single-cell transcriptome analysis of tumor immune micro-environment characteristics in colorectal cancer liver metastasis. *Ann. Transl. Med.* **2022**, *10* (21), 1170 DOI: 10.21037/atm-22-5270.

(73) Kolev, Y.; Uetake, H.; Iida, S.; Ishikawa, T.; Kawano, T.; Sugihara, K. Prognostic significance of VEGF expression in correlation with COX-2, microvessel density, and clinicopathological characteristics in human gastric carcinoma. *Ann. Surgical Oncol.* **2007**, *14*, 2738–2747.

(74) Saeed, A.; Park, R.; Sun, W. The integration of immune checkpoint inhibitors with VEGF targeted agents in advanced gastric and gastroesophageal adenocarcinoma: a review on the rationale and results of early phase trials. *J. Hematol. Oncol.* **2021**, *14*, 1–11.